University of Potsdam
Institute of Earth and Environmental Science

—

Helmholtz-Centre Potsdam
GFZ German Research Centre for Geosciences

MASTER THESIS

Implementation of a snow routine into the hydrological model WASA-SED and its validation in a mountainous catchment

Master Program
Geoecology

Erwin Rottler
Matriculation number: 759715

November 2017

1. Supervisor: Dr. Till Francke
2. Supervisor: Dr. Abror Gafurov

Published online on the
Publication Server of the University of Potsdam:
https://doi.org/10.25932/publishup-50496
https://nbn-resolving.org/urn:nbn:de:kobv:517-opus4-504963

Contents

List of Figures

List of Tables

Summary

In many regions of the world, snow accumulation and melt constitute important components of the hydrologic cycle (Gray and Prowse, 1993). With the objective to improve model performance of the hydrological model WASA-SED (Water Availability in Semi-Arid environments - SEDiments) in catchments affected by snow and ice, a physically-based snow routine has been implemented into the model. The snow routine bases on the energy-balance method of the ECHSE (Eco-hydrological Simulation Environment) software. A first test application has been conducted in two sub-basins of the Isábena river catchment (Central Spanish Pre-Pyrenees). Results were validated using satellite-derived snow cover data. Furthermore, a rainfall gauge correction algorithm to restore the liquid precipitation signal of measurements affected by solid precipitation was applied. The snow module proved to be able to capture the dynamics of the snow cover forming during the cold months of the year. The temporary storage of water in the snow cover is able to improve simulations of river discharge. General patterns of the temporal evolution of observed and simulated snow cover fractions coincide. The work conducted only represents a first step in the process of implementation and evaluation of a physically-based snow routine into WASA-SED. Future work is necessary to further improve and test the snow routine and to resolve difficulties that occurred during model applications in the catchment.

Zusammenfassung

In vielen Gebieten der Erde stellen die Prozesse Schneeakkumulation und -schmelze einen wichtigen Bestandteil des Wasserkreislaufs dar (Gray and Prowse, 1993). Im Bestreben, Simulationen des hydrologischen Modells WASA-SED (Water Availability in Semi-Arid environments - SEDiments) in Gebieten mit Schnee und Eis zu verbessern, wurde eine physikalisch basierte Schneeroutine in die Modellstruktur implementiert. Die Schneeroutine beruht auf der Energiebilanz-Methode der ECHSE-Software (Eco-hydrological Simulation Environment). Eine erste Anwendung wurde in zwei Teileinzugsgebieten des Flusses Isábena (zentrale, spanische Pre-Pyrenäen) durchgeführt. Die Validierung der Ergebnisse erfolgte anhand satellitengestützter Schneebedeckungsdaten. Außerdem wurde ein Korrekturalgorithmus zur Wiederherestellung des Signals flüssigen Niederschlags angewendet. Die Schneeroutine konnte die Dynamik der winterlichen Schneedecke erfassen. Die temporäre Speicherung des Niederschlags in der Schneedecken konnte Simulationen des Abflusses im Gebiet verbessern. Das generelle Muster der zeitlichen Entwicklung simulierter und beobachteter Schneebedeckungsgrade stimmt überein. Die durchgeführte Arbeit ist nur ein erster Schritt im Prozess der Implementierung und Validierung einer physikalisch begründeten WASA-SED Schneeroutine. Zukünftige Forschungsarbeit ist nötig, um die Schneeroutine weiter zu verbessern, zu testen und aufgetretene Schwierigkeiten bei der Modellanwendung im Gebiet zu lösen.

1 Introduction

1.1 Starting point

> "In mountainous areas where snow is a significant part of the hydrologic cycle, snowmelt is a primary water input to the soil and stream system. It is, therefore, essential to simulate snow accumulation and melt accurately" (Garen and Marks, 2005).

1.2 WASA-SED

1.2.1 Model development

WASA (Water Availability in Semi-Arid environments) is a continuous, deterministic, spatially semi-distributed hydrological model, originally developed by (Güntner, 2002) in the attempt to quantify water availability in semi-arid regions. In order to enable simulations of water transport and storage under historical and future conditions, process-oriented conceptual approaches were chosen to build the model components of WASA. All model components respect the specific conditions prevailing in semi-arid areas. Particular focus is on the surface processes evapotranspiration and infiltration-excess runoff including lateral interactions (Güntner, 2002).

Ever since the first set up, WASA is subject to the process of advancement and expansion. One important expansion is the implementation of a sediment routine into the WASA framework. The sediment routine provides numerical approaches to determine sediment generation and transport in the hillslope, transport and retention in the river network and a separate reservoir module to account for reservoir sedimentation (Mueller et al., 2010). In the course of this model extension, the WASA model was renamed WASA-SED (Water Availability in Semi-Arid environments – SEDiments). A detailed description can be found in (Mueller et al., 2010). It should be noted that sediment dynamics are not modeled in the framework of this study. Hereafter the focus is on the hydrological model part of WASA-SED.

1.2.2 Hillslope-based landscape discretisation

To be able to "represent the dominant processes in semi-arid regions at their specific scale while linking these process scales with the final scale" (Güntner and Bronstert, 2004) a semi-distributed approach based on hillslopes was developed along with WASA model (Güntner and Bronstert, 2004).

Based on this concept of an hierarchical top-down disaggregation of a landscape Francke et al. (2008) developed the software tool LUMP (Landscape Unit Mapping Programm). For the first time an objective and easily reproducible preparation of spatial data for semi-distributed, hillslope-based models is possible (Francke et al., 2008; Mueller et al., 2010). The recently published computer software lumpR described in Pilz et al. (2017) represents a further step towards an user-friendly, easy accessible and efficient mapping tool for hillslope-based landscape discretization.

In the following, a short overview on this hierarchical multi-scale landscape discretization scheme based on descriptions in Güntner and Bronstert (2004) and Francke et al. (2008) is given. In total six interlinked spatial scale levels can be distinguished. First of all, the study area is divided into sub-basins. Next step is the partitioning of those sub-basins into areas of landscape units (LU). In order to achieve this, the whole area is sub-divided into elementary hillslope areas (EHA), the basic unit for the delineation of LUs (Francke et al., 2008). One can picture EHAs as small subcatchments stringed together along the hillslope draining into the associated downslope river channel (Garbrecht and Martz, 2000; Francke et al., 2008). Using characteristics of the representative hillslope profile of an EHA, such as horizontal and vertical length and the shape of the hillslope profile, all EHAs are grouped into a given number of classes using cluster analysis (Francke et al., 2008). EHAs of one class form a LU and from now on are characterized by a representative toposequence. The toposequence extends from the channel up to the local divide. LUs represent the last spacial scale with geographically referenced locations. On finer scales only areal fractions and relative locations are used. Next, the representative toposequence of each LU is sub-divided into terrain components (TC). Important characteristics of a TC are the mean slope, its relative position to other TCs and attributes such as the occurrence of a specific soil type or vegetation class (Francke et al., 2008; Güntner and Bronstert, 2004). TCs are further

sub-divided into soil-vegetation components (SVCs). The introduction of this scale level attempts to address heterogeneity of soil and vegetation within a TC. The hierarchical top-down disaggregation is completed by the definition of the smallest scale, the representative soil profiles for each SVC. Compared to raster-based approaches this hillslope-based disaggregation of a landscape preserves process-relevant spatial variations along the hillslopes. The aggregation of land area in the different levels of the hierarchy guarantees low computational effort, even for large river basins (Francke et al., 2008; Güntner and Bronstert, 2004).

1.2.3 Process representation and chronology of computations

The temporal sequence of computations of the different hydrological processes within the multi-level representation of the landscape follow a certain order. A full description of the hydrological model components and more detailed information on the order of computations can be found in Güntner (2002) and (Mueller et al., 2010).

Computations start at the highest located TC of a LU and are performed for all SVCs within this TC. First, soil moisture is updated with the lateral subsurface inflow from the previous time step. This lateral subsurface inflow originates from the upslope located TC and from other SVCs within the same TC. Once the soil profile is saturated, additionally added water becomes surface runoff. As soon as the soil moisture is updated, processes related to precipitation are addressed. Interception storage, interception evaporation and possible saturation-excess surface runoff are calculated. Interception of rainfall on plant surfaces is modeled using a simple bucket approach (Güntner, 2002). Evaporation from the interception storage is calculated using the Penman-Monteith equation (Monteith, 1965). Is the interception storage full, additional rainfall reaches the soil surface directly. Infiltration of precipitation reaching the soil surface and possible lateral surface flow from other SVCs or the upslope located TC is determined on the basis of the Green-Ampt approach (Green and Ampt, 1911) with adaptions of Peschke (1977, 1987) and Schulla (1997). Simultaneously, possible infiltration-excess and saturation-excess surface runoff is determined.

Before plant transpiration and evaporation from the soil surface is calculated,

the soil moisture is updated again. Güntner (2002) selects a one compartment, two layer model to calculate evaporation from the soil and the transpiration of plants (Shuttleworth and Wallace, 1985). This approach assumes the canopy cover to be continuous and bare soil and vegetation to be two interrelated source layers. The evaporation from open water bodies is, similar to evaporation from the interception storage, calculated with the Penman-Monteith equation (Monteith, 1965). After, the soil moisture of all horizons is updated again. As a next step, vertical water fluxes within the soil and lateral subsurface flows to other SVCs or the downsloap located TC are determined and the soil moisture updated once more. In LUs where groundwater is assumed a significant contributor to streamflow, water that leaves the soil zones is collected in a conceptual groundwater body. A constant fraction of the input is assumed to evaporate. The remaining groundwater either is lost to deep groundwater or contributes to the river network following a simple linear storage approach (Güntner, 2002).

At the end of the computations for a TC, the saturated fraction of the SVCs and the total lateral outflow is determined. This outflow ends up either in the river network or as inflow in the downslope located TC. All steps are repeated for all SVCs of the downslope located TC. Computations of soil moisture dynamics and runoff generation for one time step are completed once all TCs of all LUs are processed. Runoff routing in the river network can be assessed using a linear response function (Güntner, 2002) or a kinematic wave approximation after Muskingum (Mueller et al., 2010). The river network is assumed to be composed of individual river stretches. Each stretch receives water fluxes from the adjoining sub-basin and the upstream river network (Mueller et al., 2010). Small and medium-sized reservoirs, often very frequent in semi-arid regions, are addressed using a cascade routing scheme. For large reservoirs the water balance is calculated individually (Güntner, 2002).

1.2.4 Demand for snow and ice

Initially developed for the application in the semi-arid north-east of Brazil, WASA does not account for the presence of snow or ice. However, in many semi-arid catchments, particularly regions enclosing high mountain ridges, snow accumulation and

snow and glacier melt constitute important hydrological processes. In general, two categories of melt models can be distinguished: empirical temperature-index models and physically-based energy balance models. Physically-based approaches simulate the energy balance to predict melt (Garen and Marks, 2005). Temperature index models base on an assumed relationship between melt and air temperature. A factor of proportionality, usually referred to as for example degree-day factor or melt factor, depending on the exact approach, relates air temperature and melt (Hock, 2003). Particularly due to the simplicity and the low data requirements, temperature index methods are widely used in snow and glacier modeling (Hock, 2003).

1.3 WASA-ALPINE

1.3.1 Process representation

In order to use the WASA model in mountainous catchments influenced by snow and ice, the hydrological part of WASA was extended by routines for snow accumulation and snow and glacier melt based on temperature-index approaches (Duethmann et al., 2013, 2014, 2015, 2016). In the following, the WASA model extended for mountainous regions with snow and glacier melt based on the temperature index method will be revered to as WASA-ALPINE. A detailed description including equations of the modifications of the WASA model in the framework of this extension can be found in Duethmann et al. (2015).

Within this extension, precipitation is treated as liquid or solid based on a calibrated threshold temperature. A sinusoidal modification of the melt factor during the course of a year, with minimum values at the winter solstice and maximum values at the summer solstice, reflects intra-annual variations of incoming solar radiation and snow albedo (Duethmann et al., 2014). The spatial variability of snow due to, for example spatial variability of precipitation, wind drift or variability in the melt process, is represented using a snow depletion curve. The fractional snow cover area is determined as a function of the snow water equivalent divided by the maximum snow water equivalent at the end of the accumulation season (Duethmann et al., 2015). The determination of fractional snow cover allows the inclusion of satellite-derived snow cover data into the model calibration process. This rep-

resents an opportunity to improve hydrological model applications, particularly in remote mountainous catchments (Duethmann et al., 2014). To avoid snow accumulation over several years outside glaciated areas, snow is redistributed to lower elevations when the snow water equivalent crosses a threshold of 3 m. This modification accounts for downhill snow transport by avalanches or wind (Duethmann et al., 2015).

1.3.2 HRU-based spatial discretisation

This extension of WASA for mountainous regions goes along with the usage of hydrological response units (HRUs) delineated based on 200 m elevation bands, instead of a hillslope-based spatial discretization (Duethmann et al., 2015). The spatial discretisation based on elevation bands introduced within WASA-ALPINE helps to keep computational time low and customizes the model to the conditions in high-elevation regions dominated by snow and ice.

1.3.3 Limitations and alternatives

WASA-ALPINE constitutes a successful WASA model extension for snow and glacier dynamics. However, the deviation from the initial spatial concept based on hillslopes developed along with the WASA model itself, poses a drawback for model applications with focus on river and sediment transport. The abandonment of the hillslope-based discretisation approach in favor of snow and ice simulations seems not to be suitable for applications in catchments outside high-elevation regions. To extend the usability of WASA-SED to semi-arid regions with influence of snow and ice, the model still is in need for an appropriate representation of snow accumulation and snow and glacier melt.

Besides temperature-index models, physically-based approaches are available to fulfill this task. In general, energy balance melt models apply the principles of conservation of energy and mass. Physically-based approaches often are put aside on the grounds of too extensive data requirements. However, with increasing computer power and the understanding that "snowmelt can be simply and reliably modeled with a physically-based energy budget using no more data than required for most temperature-index methods" (Walter et al., 2005), melt modeling based

on the energy equation receives more and more attention. Energy balance models are better suited to capture the spatial and temporal variability of melt processes (Hock, 2003). Particularly in model applications with high temporal resolution and during extreme situations, for example rain on snow events or situations when net radiation and latent heat energy are large, and air temperature low, physically-based approaches outperform empirical approaches (Hock, 2003; Gray and Prowse, 1993). Furthermore, physically-based methods provide the possibility to identify sources of errors using available process insights (Walter et al., 2005).

1.4 Aims and objectives

On the basis of the above presented concepts and needs, the main objective of this study is the implementation of a physically-based snow-routine into WASA-SED and its validation in a mountainous catchment. The implementation represents an important step in the process of advancement and expansion of WASA. The snow routine implemented in the framework of this study aims to primarily simulate the dynamics of a seasonal snow cover. Glacier melt is not considered. In the following, the WASA-SED model extended for snow accumulation and melt using a physically-based energy balance approach will be revered to as WASA-SNOW. The model is validated in the headwaters of the Isábena river catchment (Central Spanish Pre-Pyrenees). Furthermore, to correct rainfall measurements affected by solid precipitation, a new precipitation gauge correction method is presented and applied. Corrected rainfall input data is used to investigate the question whether rain gauge measurement devices itself function as precipitation pre-processing tool by storing and melting snow in its collector device. Different model variants are compared according to their ability of simulating measured discharge. Satellite-derived snow cover data is used to assess internal consistency of model runs.

2 Material and Methods

2.1 WASA-SNOW

2.1.1 Description snow routine

The snow routine implemented in the framework of this study bases on the energy balance method of the ECHSE (Eco-hydrological Simulation Environment) software. ECHSE is an open source modeling framework with a "lightweight infrastructure for the rapid development of new, re-usable simulation tools" (Kneis, 2015) for hydrological catchment modeling. For more information and access to the documentation and source codes of ECHSE visit the project website `echse.github.io`. The most important characteristics of the snow routine implemented in WASA-SNOW are described in the following section. A detailed documentation, including all equations can be found in (Kneis, 2012).

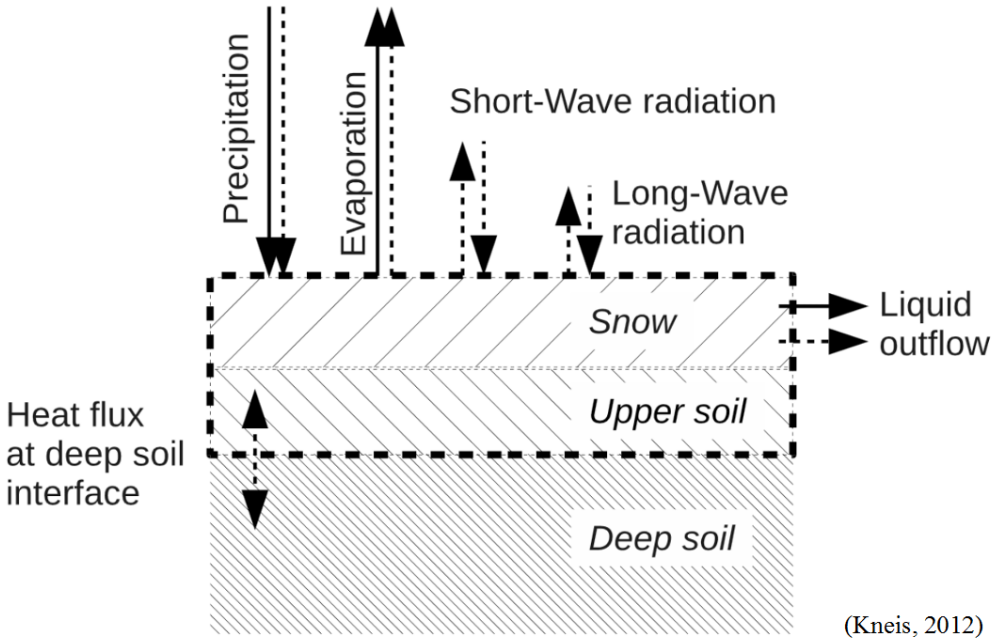

Figure 1: Fluxes of mass (solid arrows) and heat (dashed arrows)

Snow water equivalent SWE and snow energy content SEC are defined as primarily state variables. The snow energy content is determined relative to the reference state of water in the ice phase at 0°C. Furthermore, snow albedo is con-

sidered an auxiliary state variable. The dynamics of SWE and SEC are controlled by mass and energy balance, respectively. The coupling of mass and energy fluxes is illustrated in Fig.1. The snow cover is treated as one homogeneous layer. To account for thermal interactions with the ground on short time scales, the upper soil layer and the snow cover are treated as single system (Kneis, 2012). The depth-average temperature T_s is calculated using the state variables SWE and SEC:

$$T_s = \frac{SEC}{SWE \times \rho_w \times C_{ice} + D_s \times \rho_s \times C_s} \tag{1}$$

where ρ_w is the density of water, C_{ice} the specific heat of ice, D_s the depth of the upper soil, ρ_s the soil density and C_s the soil's specific heat capacity. At positive SEC, when snow is melting, T_s is set to 0°C. The snow surface temperature T_{ss}, which is important for computations of energy flux components at the snow-atmosphere interface, is estimated from T_s and the air temperature T_a using the weighting parameter μ:

$$T_{ss} = (1 - \mu)T_s + \mu T_a \tag{2}$$

T_{ss} cannot become greater than 0°C. A threshold temperature T_{crit} defines, whether precipitation input gets treated as rain or snow. Changes in SWE depend on mass input by precipitation and mass loss from meltwater outflow and sublimation. The melt water outflow M_{flow} is assumed to equal the snow cover's actual hydraulic conductivity. The actual hydraulic conductivity is calculated using the saturated hydraulic conductivity $k_{sat,snow}$ and the relative saturation of the snow RSS.

$$M_{flow} = k_{sat,snow} \times RSS^3 \tag{3}$$

RSS is a measure for the availability of liquid water and "is defined as the relative saturation in excess of water retained by capillary forces" (Kneis, 2012):

$$RSS = \frac{\text{liquid vol. - capillary retention vol.}}{\text{pore vol. - capillary retention vol.}} \tag{4}$$

For more information see also Illangasekare et al. (1990) and Tarboton and Luce (1996). When relating the capillary retention volume to the SWE, the equation

can be rewritten as:

$$RSS = \frac{\frac{SLF}{1-SLF} - SCR}{\frac{\rho_w}{\rho_{snow,dry}} - \frac{\rho_w}{\rho_i} - SCR} \tag{5}$$

where SLF is the fraction of liquid water in the snow cover, SCR the capillary retention volume related to the solid part of the SWE, $\rho_{snow,dry}$ the density of dry snow and ρ_i the density of ice. SCR is assumed constant (Tarboton and Luce, 1996). SLF represents a mass fraction and can be computed using the equation:

$$SLF = \frac{SEC}{SWE \times \rho_w \times H_{ice}} \tag{6}$$

where H_{ice} is the latent heat of ice fusion (melt heat). The sublimation mass flux M_{subl}, the mass loss through solid-gaseous phase transition, is determined assuming a proportional relationship between M_{subl} and the gradient between the specific humidities aboveq q_a and at the snow surface q_s as described in Tarboton and Luce (1996) and Dyck and Peschke (1995).

$$M_{subl} = D \times \frac{\rho_a}{\rho_w} \times (q_s - q_a) \tag{7}$$

The development of the snow albedo (AS) is described with a simple aging approach presented in Dyck and Peschke (1995). This approach allows to account for the general decrease of AS due to processes such as metamorphism and pollution (Kneis, 2012). Each time snow falls, AS is reset to its previously defined maximum value AS_{max}.

$$G_{alb} = k_{AS}(T_a) \times (AS_{min} - AS) \tag{8}$$

with G_{alb} being the process rate controlling the albedo change, k_{AS} the aging rate and AS_{min} the minimum albedo for old snow. Two different k_{AS} are distinguished depending whether T_a is positive or negative. Changes in SEC are determined based on calculations of the shortwave radiation balance R_{netS}, the longwave radiation balance R_{netL}, soil heat fluxes R_{soil}, sensible heat fluxes R_{sens} and energy changes due to precipitation, sublimation and melt fluxes. The short- and longwave radiation balances are calculated as follows:

$$R_{netS} = SR \times (1 - AS) \tag{9}$$

$$R_{netL} = R_{inL} - R_{outL} \tag{10}$$

SR is the incoming solar radiation. R_{netL} is the difference between incoming R_{inL} and outgoing R_{outL} long-wave radiation. The outgoing long-wave emissions of the snow pack are determined according to the Stefan-Boltzmann equation:

$$R_{outL} = \epsilon \times \sigma \times (T_{ss} + 273.15)^4 \tag{11}$$

where ϵ is emissivity of the snow pack and σ the Stefan-Boltzmann constant. The emissivity is dynamically computed using the auxiliary state variable AS:

$$\epsilon = \epsilon_{min} + (\epsilon_{max} - \epsilon_{min}) \times \frac{AS - AS_{min}}{AS_{max} - AS_{min}} \tag{12}$$

with ϵ_{min} and ϵ_{max} being the minimum and maximum snow emissivity for old and new snow. Within the incoming part of the long-wave radiation balance, clear sky $R_{inL,cs}$ and cloud emission $R_{inL,cl}$ are distinguished and weighted using the cloud cover fraction (FC).

$$R_{inL} = (1 - FC) \times R_{inL,cs} + FC \times R_{inL,cl} \tag{13}$$

$R_{inL,cs}$ and $R_{inL,cl}$ both are computed using the Stefan-Boltzmann equation. For $R_{inL,cs}$ temperature is set to T_a. The developer of ECHSE selected an empirical formula developed by Brund relating clear-sky emissivity and vapor pressure to estimate the emissivity (see Hock (2005)). Clouds are assumed black bodies with an emissivity of one. The cloud temperature is approximated by the dewpoint temperature. The sensible heat flux at the snow-atmosphere is calculated using an equation presented in Tarboton and Luce (1996) and Dyck and Peschke (1995):

$$R_{sens} = D \times \rho_a \times C_{air} \times 10^3 \times (T_a - T_{ss}) \tag{14}$$

where D is a turbulent transfer coefficient, ρ_a the density of air and C_{air} the specific heat capacity of air. Within this approach R_{sens} is assumed proportional to the

temperature gradient between atmosphere and snow surface. D is estimated based on a linear approach developed by Knauf (1980):

$$D = a_0 + a_1 \times WS \tag{15}$$

where a_0 and a_1 are dimensionless empirical coefficients and WS wind speed. R_{soil} is defined as the long-term average flux into the deep soil and set to 0, if not known. Conversion factors for precipitation, sublimation and meltwater outflow are used to relate mass and energy fluxes.

2.1.2 Practical realization of implementation

2.1.2.1 Standalone verion: snowAlone

As a first step of the implementation process, the snow model from ECHSE, written in C++, was rewritten as a standalone Fortran Console Application. This standalone version of the snow routine, subsequently revered to as snowAlone, consists of the four Fortran script files snow_standalone, snow_compute, read_snow_params and snow_h. The file snow_standalone contains the main program and provides the environment from whom the subroutine snow_compute is called. The subroutine snow_compute contains all equations needed for the calculations of the dynamics of the snow cover. Within snow_h variables for the parameters used in the model are declared. The parameters are read from the external input file snow_params using the subroutine defined in the file read_snow_params.

snow_compute and the parameter file snow_params form the core of the snow model. snowAlone and WASA-SED call upon the same core for calculations of snow cover dynamics (Fig.2). The slim design of snowAlone enables fast development and testing of the snow model.

2.1.2.2 Precipitation pre-processing

Next step in the process of implementation is the integration of the snow routine into the WASA-SED environment. The WASA-SED program is large and complex and consists of numerous individual source files. The folder system of the WASA-SED code reflects the three conceptual levels of the model. The three

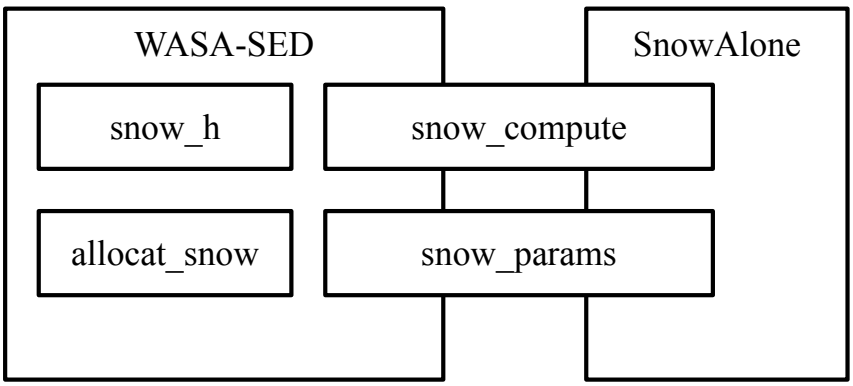

Figure 2: Source code structure snowAlone and snow routine WASA-SED

levels hillslope scale, river scale and reservoir scale each has its individual folder with corresponding files. In the framework of this work, the snow routine is assumed to only affect processes on the hillslope scale. Source code of the model compartments river and reservoir remain unchanged. The snow routine is considered a pre-processing tool of the incoming precipitation signal. When the air temperature falls below T_{crit}, rainfall is treated as snow and stored in the snow pack. Precipitation leaves this intermediate storage as melt water outflow. The modified precipitation signal subsequently enters the model compartment of interception and the modeling of processes continuous according to the temporal sequence described in section 1.2.3. If there is no snow present, neither accumulated on the surface nor precipitation falling as snow, the precipitation signal remains unchanged. Regarding code structure, the subroutine snow_compute is called within the hydrological subroutine soilwat, which computes water and sediment balances for the terrain components. The parameter input file snow_params is read in within the subroutine readgen. Two more source files were added to the existing WASA-SED code to complete the implementation, the files allocat_snow and snow_h. Within snow_h all variables related to the snow routine are declared and additional subroutines and functions related to the snow module stored. The purpose of the file allocat_snow, which is called once at the beginning of a sim-

ulation within the subroutine readhymo, is to allocate all variables related to the snow routine and to calculate the relative elevation of TCs. It should be noted, that the source file snow_h of WASA-SED is different to the source file snow_h of the standalone version snowAlone. Similar names had to be declared to ensure compatibility of the core.

2.1.2.3 Relative elevation

So far, information on elevation of TCs is not available in WASA. This information gets lost in the process of the hillslope-based landscape discretization. However, using the available characteristics of LUs and TCs, it is possible to determine a relative elevation. This relative elevation of a TC is defined as the relative height of a center of a TC to the mean elevation of the sub-basin. First, available information on slope of the TC, fraction of the TC within the toposequence, and length of the toposequence are used to determine the relative elevation of a TC within its LU. Fig.3 illustrates a simple example with a toposequence composed of three TCs of 200 m vertical extend. To complete the calculation of the relative elevation of a TC, the relative elevation of the associated LU is added. Information on the relative elevation of a LU recently became available in WASA. The developers of WASA and lumpR integrated calculations of relative elevation and aspect of LUs into the lumpR software. The new variables are stored and read in from the new input data file lu2.dat.

2.1.2.4 Elevation dependent temperature adjustment

The relative elevation of a TC is used in the subroutine snow_prepare_input, located in snow_h, to enable modifications of temperature according to their elevation using a simple lapse-rate-based approach. Meteorological input is assumed uniform on sub-basin scale. This modification is an attempt to address for altitude dependency of meteorological input. A simple example of the modification of temperature along the hillslope is illustrated in Fig.3. The original temperature input value of 0 °C is modified by an for this example used temperature lapse-rate of -1 °C/100m. For the Isábena case study area, temperature is assumed to decrease with elevation according to a lapse rate of 0.6 °C/100m (Fig.16). This value was

derived analyzing available temperature data of the region. The temperature lapse rate is read in from the snow routine parameter file snow_params.

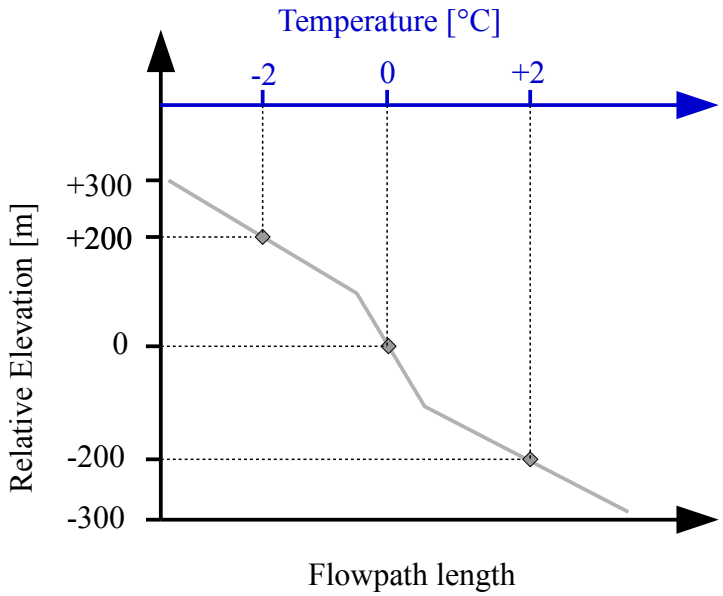

Figure 3: Elevation dependent temperature adjustment

2.1.2.5 Radiation modification for aspect and slope

Recently, the developers of WASA extended the program code for equations enabling the correction of the radiation input signal according to aspect and slope. This new feature is used to modify the radiation input signal of the snow routine. As there is no detailed description of this new feature available yet, the following section attempts to give a first insight into this model component describing the calculations during a model run in daily resolution. All angels used in the following equations are given in radians. During a model run in daily resolution the modification approach returns daily and hourly values of radiation corrected for aspect and slope.

As a first step, values of hourly extraterrestrial radiation I_0 are calculated based on equation (1) presented in Allen et al. (2006):

$$I_0 = S_0 \times E \times \cos(\theta) \tag{16}$$

where S_0 is the solar constant, E an eccentricity correction factor and θ the angle of incidence onto a horizontal surface at the location of interest. The eccentricity correction factor is computed using equation A.2 in Tian et al. (2001):

$$E = 1 + 0.033 \times \cos(\frac{2d_n}{365}) \tag{17}$$

where d_n is the day number of the year. The solar incidence angle onto a horizontal surface is determined using equation (4) in Allen et al. (2006):

$$cos(\theta) = \sin(\delta)sin(\phi) + \cos(\delta)\cos(\phi)\cos(w) \tag{18}$$

where δ is the declination of the earth, ϕ the latitude of the location and w the hourly angle. The latitude is read in from the control file snow_params. Latitude and longitude values are given in degree in the control file and are converted to radians during read in. The hourly angle "is the angular distance between the observer's meridian and the meridian whose plane contains the sun" (Maleki et al., 2017) and is calculated using the equation from Maleki et al. (2017), page 3:

$$w = 15(12 - ST) \tag{19}$$

where ST is the local solar time. Next, the hourly extraterrestrial values are re-scaled to fit surface radiation values using the re-scaling factor K_t presented as daily 'clearness index' in Maleki et al. (2017). This index is defined as the ratio of measured radiation values at the earth's surface to extraterrestrial values. Extraterrestrial radiation in daily resolution H_0 is calculated using the equation:

$$H_0 = \frac{24 \times 3.6}{\pi} S_0 E \times (\sin(\delta)\sin(\phi)w + \cos(\delta)\cos(\phi)\sin(w_s)) \tag{20}$$

where w_s is the sunrise hour angle (Maleki et al., 2017). The sunrise hour angle w_s is calculated using equation A.5 from Tian et al. (2001):

$$\cos(w_s) = \arccos(-\tan(\phi)\tan(\delta)) \tag{21}$$

The hourly global radiation onto a horizontal plane G_h, re-scaled using daily radiation measurements, is determined using following equation:

$$G_h = I_0 \times K_t \tag{22}$$

Next and final step in the correction process is the derivation of the solar irradiance for an inclined plane G_d. Therefore, direct G_b and diffuse G_d radiation components are distinguished according to the approach presented inTian et al. (2001):

$$G_d = G_b + G_d \tag{23}$$

The direct radiation component is determined based on equation (1) presented in Hay and Mckay (1985):

$$G_b = S_0 \times E \times K_t \times (1 - K_r) \times \cos(\theta_s) \tag{24}$$

where K_r is the fraction of global radiation that is diffuse and θ_s the angle of incidence on the inclined surface. K_r is attained using a semi-empirical linear approach similar to equation (1) in Tian et al. (2001). Parameters for selected linear method were determined using the Reindl-1 model to estimate diffuse radiation as described in Maleki et al. (2017). θ_s was determined using corresponding equation described in Garnier and Ohmura (1968) and Duffie and Beckman (1980) and presented as equation (3) in Allen et al. (2006):

$$\begin{aligned} cos(\theta_s) = {} & sin(\delta)sin(\phi)cos(s) \\ & - \sin(\delta)\cos(\phi)\sin(s)\cos(\gamma) \\ & + \cos(\delta)\cos(\phi)\cos(s)\cos(w) \\ & + \cos(\delta)\sin(\phi)\sin(s)\cos(\gamma)\cos(w) \\ & + \cos(\delta)\sin(\gamma)\sin(s)\sin(w) \end{aligned} \tag{25}$$

where s is the slope of the surface and γ the surface aspect angle. Allen et al. (2006) defines the hourly angle w to be negative in the morning and positive in the afternoon. To use the definition of w from Maleki et al. (2017) (eqn. 19),

the sign of w has to be changed. The diffuse irradiation on the inclined surface is obtained using equation (2) from Tian et al. (2001):

$$G_d = G_h * (f_\beta \times K_r + 0.2 \times (1 - f_\beta)) \tag{26}$$

where f_β is the slope reduction factor defined as "the proportion of the hemisphere that is blocked by the horizontal (infinite) plane" (Tian et al., 2001). It is determined as $f_\beta = (1 - s/180)$, where s is the slope of surface. The correction process of radiation provides hourly global radiation values corrected for aspect and slope for each TC. The daily value is computed as mean of the hourly values. The radiation correction for aspect and slope was integrated into the subroutine snow_prepare_input in the source file snow_h.

2.1.2.6 Intermediate time steps

To avoid instabilities in the melting process caused by coarse time resolutions, the snow routine runs in intermediate time steps. Test runs in daily resolution revealed erratic behavior of the snow melt process when only few snow is left. In the case of a WASA-SED run in daily resolution, the snow routine currently runs in 24 intermediate time steps. The daily mean input temperature is then modified assuming sinusoidal diurnal temperature variations. Amplitude and offset of the sine wave can be specified by the user and are read in from parameter file snow_params. Offset is given by the deviation of the daytime maximum temperature from noon 12:00 pm. In the framework of this study an daily temperature amplitude of 8°C and and offset of +2h was selected. Temperature input for the intermediate time steps from an for example daily mean temperature input of -2°C, vary between -6°and 2°C with maximum temperature at the the time step representing 2pm (Fig.4). Short-wave radiation input for the intermediate time steps of the snow routine is taken from the radiation correction presented in section 2.1.2.5. Rainfall input is equally distributed among the hourly intermediate time steps.

The usage of intermediate time steps in model runs with coarse time resolution also improves model performance in cases of rain on snow. Rainfall on a snow cover adds both mass and energy in the present time step. Melt water outflow due to the energy input by rainfall occurs in the following time step. During extreme

events with flood generation accompanied or caused by rainfall this offset between rainfall event and melt due to energy input by rainfall might cause inconsistencies when time resolution is too coarse.

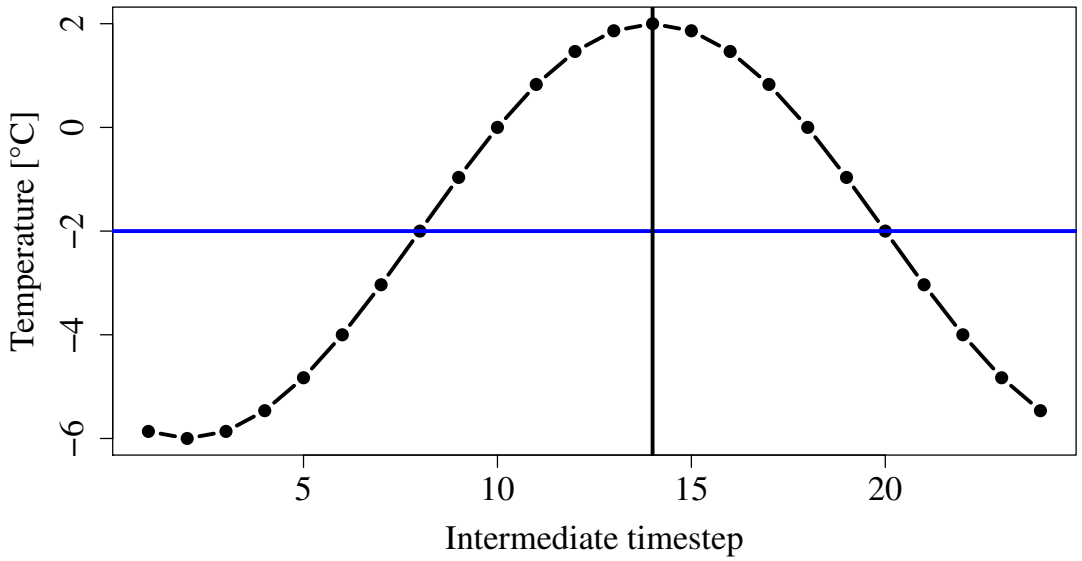

Figure 4: Sinusoidal temperature modification during daily model runs for an input temperature of -2°C, a selected temperature amplitude of 8°C and offset of the peak from 12:00 of +2h

2.1.2.7 Snow routine options

The snow routine implemented into WASA-SED in the framework of this study is an optional module. Depending on the user's needs it can be turned on or off. A corresponding logical parameter was included into the control file do.dat. This control file contains the main parameter specifications for a model run. The logical parameter is called dosnow. If set to 1, the snow routine is active and all related calculations are performed. If set to 0, the snow routine remains inactive.

Output files can be generated for all state variables and mass and energy fluxes related to the snow routine. The specification, which output file is prepared, occurs

Table 1: Keywords and descriptions optional outfiles related to the snow routine

Keyword	**Description**
snowEnergyCont	Snow energy content of snow cover [kJ/m^2]
snowWaterEquiv	Snow water equivalent snow cover [m]
snowAlbedo	Snow albedo [-]
snowCover	Snow cover [-]
snowTemp	Snow temperature [°C]
surfTemp	Snow surface temperature [°C]
liquFrac	Fraction of liquid water [-]
fluxPrec	Precipitation flux [m/s]
fluxFlow	Melt water flux [m/s]
fluxSubl	Sublimation flux [m/s]
fluxNetS	Short-wave radiation balance [W/m^2]
fluxNetL	Long-wave radiation balance [W/m^2]
fluxSoil	Soil heat flux [W/m^2]
fluxSens	Sensible heat flux [W/m^2]
stoiPrec	Conversion factor mass and energy flux precipitation [kJ/m3]
stoiSubl	Conversion factor mass and energy flux sublimation [kJ/m3]
stoiFlow	Conversion factor mass and energy flux melt water [kJ/m3]
rateAlbe	Change rate snow albedo [1/s]
precipMod	Modified precipitation signal [mm]
cloudFrac	Cloud cover fraction [-]
radiMod	Radiation signal corrected for aspect and slope [W/m^2]
temperaMod	Height-modified temperature signal [°C]
rel_elevation	Relative elevation of TC to mean sub-basin [m]

in the control file outfiles.dat. The filenames of the desired output files have to be added as keyword to activate their creation. A list of possible output files with corresponding keyword is given in Tab.1. The output is created TC-wise. For each time step, values for each TC of each LU get exported.

Furthermore, two logical parameter specified in the control file snow_params, do_rad_corr and do_alt_corr, allow controlling, whether radiation correction for aspect and slope, and height-depended temperature modifications, respectively, are applied.

2.1.2.8 Cloud cover, air pressure and wind

Information on cloud cover represents a necessary input to determine the long-wave radiation balance within the snow routine. In the incoming part, clear-sky emissions and emission by clouds are distinguished and weighted according to the degree of cloud cover (see Equation 13). Güntner (2002) implemented an approach to estimate cloudiness based on equations presented in Shuttleworth (1992) for the calculations of the potential evapotranspiration.

As no measured values are available, Güntner (2002) estimates cloud cover using measured values of short-wave solar radiation and a theoretical maximum value of radiation. Both values are available inputs within the WASA structure. Depending on the time resolution of the model run, measured short-wave radiation usually is available in daily or hourly resolution. The theoretical maximum values of radiation are currently read in as monthly mean extra-terrestrial shortwave radiation. Values are selected depending on the latitudinal position of the study area.

For the snow module not the approach implemented by Güntner (2002), but cloud fraction calculated estimated based on the 'clearness index' K_t presented in section 2.1.2.5 is used. This approach uses extra-terrestrial shortwave radiation values in daily resolution, compared to the monthly values used by Güntner (2002). Air pressure and wind are set constant to 1000 hPa and 1 m/s, respectively.

2.1.2.9 Snow cover area

A variable not specifically addressed in the ECHSE environment, but potentially very useful to improve the performance of hydrological models, is the fractional snow cover. Integration of snow cover area information into the calibration and validation process of a hydrological model can improve internal model consistency and streamflow simulations during periods affected by snow accumulation and melt (Finger et al., 2015; Roy et al., 2010; Duethmann et al., 2014).

In the framework of this study, fractional snow cover is determined on sub-basin scale based on the TC-wise output of WASA. As soon as the SWE-value of a TC is greater than 2 cm, the TC is assumed to be fully covered with snow. Taking into account all TCs of all LUs and weighting them according to their areal fraction within the sub-basin, the fractional snow cover of the sub-basin is assessed.

Table 2: Modeled sub-basins of Isábena catchment

Sub-basin	Area [km^2]	Min. Altitude [m]	Mean Altitude [m]	Max. Altitude [m]
Cabecera	145	839	1503	2696
Villacarli	38	860	1341	2371

2.2 Study area and data

2.2.1 Study area

The Isábena catchment (439 km^2) is located in the Central Spanish Pre-Pyrenees (Fig.5). A typical Mediterranean mountainous type climate shapes the hydrological processes of the region. Runoff is highly dynamic and characterized by high concentrations of suspended sediment. Previous studies point out that particularly badlands located in the upper middle of the Isábena catchment constitute hotspots of erosion (Francke et al., 2008; López-Tarazón et al., 2009). The high loads of sediment pose a risk to the downstream located Barasona Reservoir in terms sedimentation and reduction of its storage capacity (Mueller et al., 2010). This study focuses on the two headwater catchments Cabecera and Villacarli. More detailed information on the two selected sub-basins is given in Tab.2. Those two sub-basins, both including mountain tops up to more than 2000 m asl, are assumed to be particularly subject to accumulation and melt of snow.

2.2.2 Model input from hillslope-based landscape discretisation

Input files for the hillslope and river module base on the in section 1.2.2 presented hierarchical top-down disaggregation of a landscape. Together with the adjoining Ésera river catchment, the Isábena catchment constituted a key test area during the development of LUMP and WASA-SED (Francke et al., 2008; Mueller et al., 2010). A database for the area was developed along with those studies and is maintained and updated ever since by the developers. This database and the used digital elevation model (DEM) were generously provided for usage in the framework of this study. Using the already established database for the Isábena catchment, two new independent databases for the two sub-basins of interest, Cabecera and Villacarli, were prepared and used for WASA input file generation. Regarding

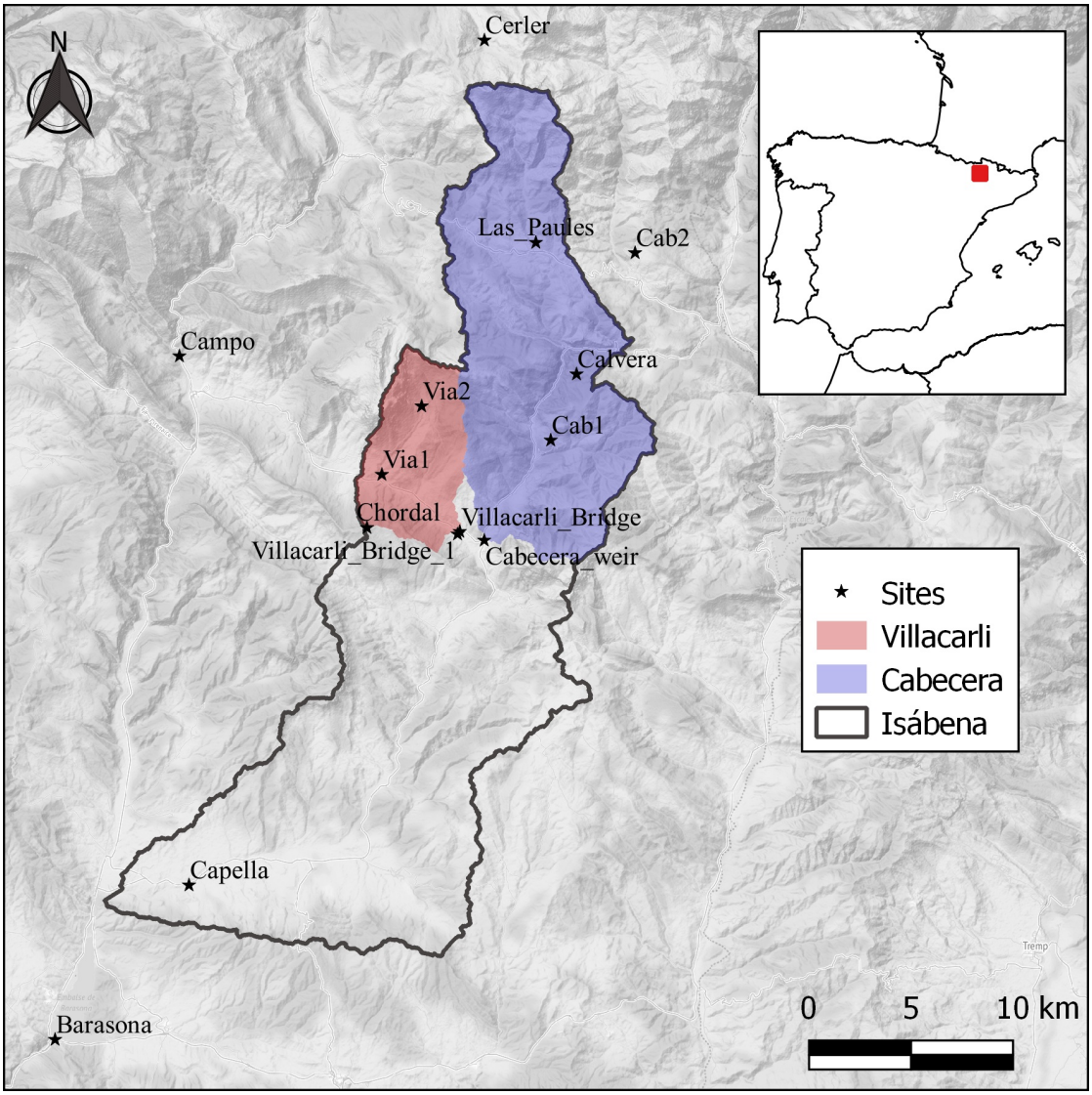

Figure 5: Topographic map of study area

relief and altitude the Ésera catchment is better suited as case study area than the Isábena river. However, several reservoirs in the river network of the Ésera river affect the measured discharge dynamics. In order to avoid possible damping effects caused by the water reservoirs, the Isábena catchment was selected.

2.2.3 Meteorological station data

All meteorological data used in this study originates from the recently within the CUAHSI Hydrological Information System published data service 'Hydro-sedimentological data Isábena, NE Spain'. All data also can be accessed via the Research Data Repository of GFZ Data Services (Francke et al., 2017b). A detailed description of the data is given in (Francke et al., 2017a). Tab.3 summarizes the most important characteristics of stations used in the framework of this study. After download, all time series were aggregated to daily values. Radiation and humidity measurements are used from the station Barasona. Barasona is the nearest site recording those variables. Values are assumed to appropriately represent the temporal dynamics of radiation and humidity for the whole area. Discharge measurements are available at the outlet of each sub-basin. For Cabecera and Villacarli river flow is measured at Cabecera_weir and Villacarli_Bridge, respectively. Data covering the time frame 01.12.2011 - 31.05.2015 was downloaded and prepared. This study focuses on the two winter periods 2013/2014 and 2014/2015. Those two periods were selected according to data availability of stations and water availability in the catchment. The winter 2011/2012 is characterized by very dry conditions making simulation results less informative. A measurement gap in the Cabecera discharge in the time crucial for snow processes of February and March during winter 2012/2013 complicate simulations of this period.

2.2.3.1 Runoff coefficients

Runoff coefficients of the two sub-basins were calculated using running sum values of rainfall and discharge with a window width of one year. Each one year window is represented by the day in the center of the period. The runoff coefficient displayed on the 1st of January, for example, represents the time frame from July of the preceding year until June of the coming year.

2.2.3.2 Precipitation gauge correction

Precipitation is a crucial input variable of hydrological models. However, quality control and correction of precipitation gauge data often only receives little attention. Tipping bucket rain gauges tend to systematically underestimate pre-

Table 3: Dataset used: SiteCode, Altitude [m], Variable(s), Latitude, Longitude

SiteCode	**Variables**	**Altitude [m]**	**Latitude**	**Longitude**
Barasona	radiation humidity	451	42.126	0.314
Cab1	rainfall	1239	42.388	0.608
Cab2	rainfall	1192	42.470	0.658
Cabecera_weir	discharge	841	42.345	0.569
Calvera	rainfall	1535	42.417	0.623
Campo	temperature	675	42.425	0.388
Capella	rainfall	490	42.193	0.394
Cerler	temperature	1900	42.563	0.568
Chordal	rainfall	1556	42.350	0.499
Las_Paules	rainfall temperature	1500	42.475	0.599
Via1	rainfall	1017	42.373	0.508
Via2	rainfall	1389	42.403	0.532
Villacarli_Bridge	temperature discharge	866	42.348	0.554
Villacarli_Bridge_1	rainfall	866	42.347	0.553

cipitation with wind-driven under-catch as the main source of error (Grossi et al., 2017; Stisen et al., 2012). In the case of liquid precipitation, this underestimation generally stays below 15% (Grossi et al., 2017). Errors can get substantially higher when precipitation falls as snow. Approaches to correct for biases in liquid and solid precipitation usually use statistical relationships based on observations of temperature and wind speed (e.g. Grossi et al. (2017); Stisen et al. (2012); Zheng et al. (2017); Sevruk (1983); Pan et al. (2016)). Precipitation data used in this study was measured by tipping bucket rain gauges with neither windshield nor heating. Measurements might be affected by wind-driven under-catch, particularly during events with solid precipitation.

As no wind speed data is available, a new correction method based on temperature data and the liquid precipitation signal from a nearby measurement site was developed and applied. In total, three time series are needed in the framework of this approach: (1) precipitation measurements affected by solid precipitation, (2) the corresponding temperature time series of this site (in the following referred

to as high station) and (3) liquid precipitation data from a nearby station (base station). First, periods during which snowfall and snow melt possibly affect the recorded precipitation at the high station are determined. The start day of such a period is identified using the following criteria: (1) the temperature at the high station is below 2°C, (2) the recorded precipitation at the base station is higher than the one recorded at the high station and (3) the precipitation recorded at the bases station is greater than 1 mm. Under conditions of temperatures below 2°C snow accumulation and snow melt are assumed to possibly affect the precipitation measurement in a significant manner. In the case of the investigated area, precipitation generally increases with altitude. Higher locations tend to record more rainfall than low lying stations. A reversed situation during cold days might be an indicator that at the high station precipitation falls as snow and cannot be recorded properly by the rain gauge. Only rainfall events grater than 1 mm, recorded at the base station, are assumed to be of importance.

The length of a snow period is determined using a simple degree day meld model. The period is extended until the possible melt exceeds the recorded rainfall at the high station. A degree day factor of 4 mm $°C^{-1}$ day^{-1}, a comparatively high value, was selected to reflect the for snow melt favorable conditions in the gauge bucket. The exposed position makes the bucket particularly vulnerable to heating through incoming solar radiation. Furthermore, a high degree day factor helps to prevent overestimation of period lengths. Once start day and length of the period are determined, the amount of precipitation measured at the high station is distributed according to the precipitation distribution of the base station within this period. The base station is assumed to receive the true liquid precipitation signal not affected by snow accumulation or melt. To account for intensified wind-driven under-catch of solid precipitation and possible blow off of accumulated snow from the bucket at the high station, the measured amount is increased by 20%. To prevent repeated correction of the precipitation signal, start days falling into the previous snow period are not considered.

Fig.6 illustrates the correction approach on a simple illustrative example case. On day one, 9 mm of rainfall are recorded at the base station, only 4 mm at the high station. In addition, recorded temperatures at the high station are below 2°C. This indicates that snow possibly affects the rainfall measurement at the high

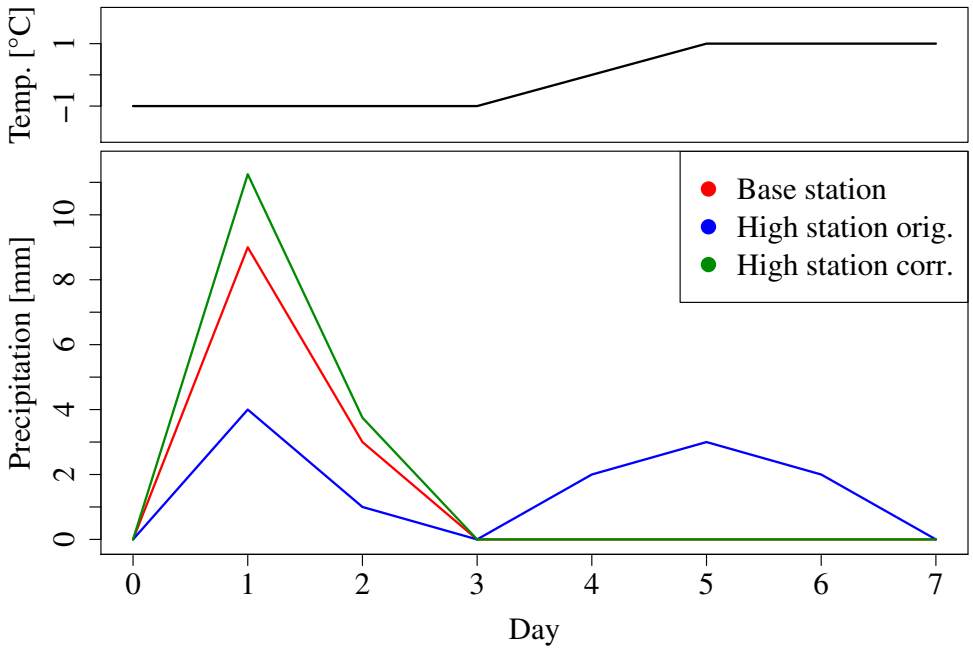

Figure 6: Precipitation gauge catch correction based on temperature and base station precipitation signal; red line represents precipitation signal of base station, blue/green line the original/corrected precipitation signal of the high station

station. Snow might be accumulated in the bucket and not measured during the event, but later during melt. This melt event might mistakenly be recorded as rainfall. The end day of this snow period is day seven. On this day, possible melt, determined using the degree day melt model, is 12 mm and equals the recorded precipitation at the high station. The 12 mm of possible melt result from three days of 1°C in combination with the selected degree day factor of 4 mm $°C^{-1}$ day^{-1}. The total amount of 12 mm recorded at the high station plus the 20% assumed loss are distributed according to the signal of the base station.

This dynamic correction approach attempts to restore the liquid precipitation signal of measurements periods affected by solid precipitation. It does not attempt to account for other sources of errors, such as wetting loss or underestimations of liquid precipitation due to wind-driven under-catch. The precipitation time series recorded at Capella is used as base station to correct at higher elevations situated rain gauges in and around the investigated sub-basins. Temperatures at Capella very seldom fall below the freezing point. Rain gauge stations investigated in the

framework of this study generally are subject to the same precipitation events, as illustrated exemplary for Capella and Via2 in Fig.7. The winter of 2012 represents an exceptional dry period and is visible in all records.

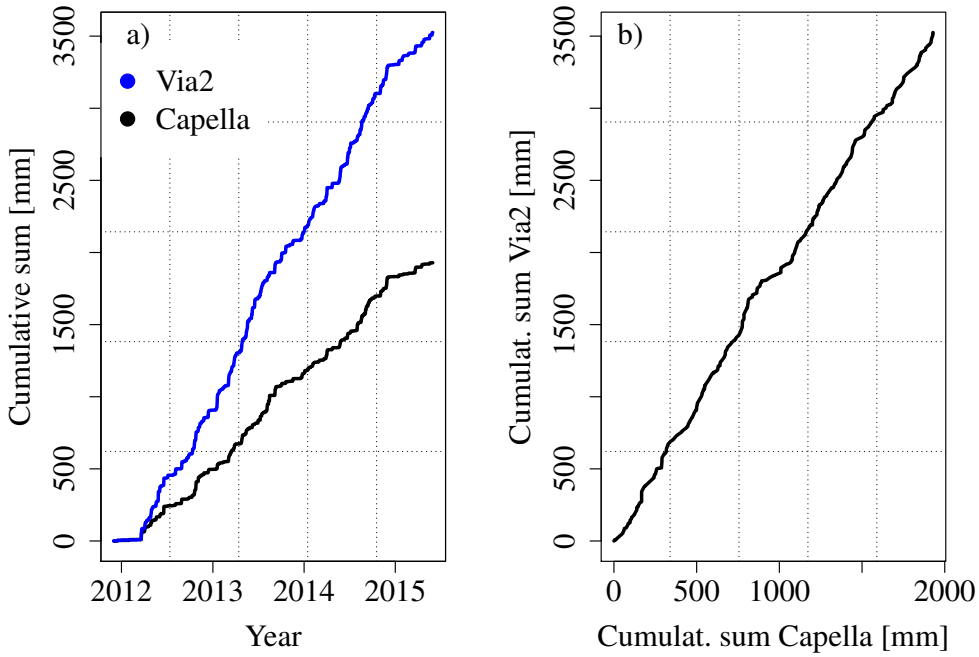

Figure 7: Rainfall station comparison: a) Cumulative sum rainfall Capella and Via2, b) direct comparison cumulative sums Capella and Via2 for the time frame 01.12.2011 - 31.05.2015

2.2.3.3 Interpolation

Temperature data is not available for all rainfall measurement sites. To be able to apply the presented precipitation correction method to all rainfall time series, temperature data was interpolated using the interpolation program 'interpol' presented in Francke (2002). The program interpolates based on an inverse-distance approach. To account for elevation differences of temperature, altitude is added as an auxiliary variable and the linear relationship between temperature and altitude computed within each time step. The height dependent adjustment is performed if the correlation coefficient of the linear regression has a value higher than 0.7.

Meteorological input to WASA-SED is on sub-basin level. To obtain repre-

sentative input time series for the each sub-basin, rainfall and temperature data was interpolated to the centroid of each sub-basin. Temperature input was interpolated in the course of interpolating to the rain gauges. The centroids were assigned the mean elevation of the corresponding sub-basin. In the case of rainfall, two independent interpolation runs were performed. The first run with the original precipitation input data, the second one with the corrected time series. Accordingly, two precipitation input time series for each sub-basin are available. Interpolation of precipitation was performed without elevation as auxiliary variable. Precipitation data from Capella was only used within the gauge correction process and not included into the interpolation runs to get the WASA-SED input time series.

2.2.4 Satellite-derived snow cover data

Moderate Resolution Imaging Spectroradiometer (MODIS) data has been shown to be an appropriate source to attain information on snow cover globally (e.g. Hall et al. (2002); Parajka and Blöschl (2006); Wang et al. (2008); Gafurov et al. (2013)). Based on the cloud removal algorithm of Gafurov and Bárdossy (2009), Gafurov et al. (2016) develop the user-friendly, all-in-one software package MODSNOW-Tool to process MODIS raw data. The package enables computations of spatiotemporal snow statistics in daily resolution and prepares cloud-free snow cover maps for a previously defined area. The developer of MODSNOW-Tool applied the software to the area of interest of this work and generously provided resulting output to be used in this study.

2.3 Model calibration

Within this study the calibration process is considered an optimization problem, as the search for the parameter set delivering best model results when comparing simulations with observed data (Tian et al., 2016; Efstratiadis and Koutsoyiannis, 2010). The idea of an optimum parameter set defined using objective functions is a widespread assumption used in calibration exercises of hydrological models (Efstratiadis and Koutsoyiannis, 2010). Different objective functions, single or multi, are available to assess model performance. Commonly used model eval-

uation methods are Nash-Sutcliff efficiency (NSE) or error indices such as the root mean square error (RMSE) (Moriasi et al., 2007). In the framework of this study RMSE was selected to asses model performance. The calibration routine applied bases on the dynamically dimensioned search (DDS) algorithm from the R-package 'ppso'. This package provides optimizing approaches using DDS and particle swarm optimization (PSO) and can be downloaded from the R-forge website (`www.rforge.net/ppso/`).

At the start of the calibration process the DDS algorithm searches globally. As the calibration procedure progresses, the algorithm automatically scales the search space according to model performance and search continues more locally (Chu et al., 2015). R-scripts performing the WASA model calibration using the 'ppso' R-package were provided by the developer of the package. This already established calibration routine was adjusted to the specific needs of this study. Model runs are calibrated using the discharge measurement at the outlet of the sub-basin. Information on fractional snow cover are not integrated into the calibration process. Instead, resulting information are used to validate internal model consistency by comparing simulated snow cover area and observed values.

During a model calibration with inactive snow routine, sets comprising factors modifying ten hydrological parameters are evaluated. Target parameters are the storage coefficient of groundwater outflow (gw_delay), thickness ($soildepth$) and saturated hydraulic conductivity ($kf\_bedrock$) of the bedrock layer located between the soil compartment and the groundwater storage, saturated hydraulic conductivity during infiltration (kf_scale), saturated hydraulic conductivity of soils ($ksat\_factor$), Muskingum river routing characteristics ($Muskingum\_X\_f$ and $Muskingum\_K\_f$), riverdepth ($riverdepth$), Manning's n of the reach of the river ($manningn$) and the hydraulic conductivity of the river bed (riv_Ksat). Expressions in brackets name the factors modifying corresponding parameters.

For model runs with active snow module, six snow parameters are calibrated in addition to the ten hydrological parameters. The six snow parameters selected for this purpose are the threshold temperature T_{crit}, the weighting parameter μ, the specific capillary retention volume SCR, the minimum snow emissivity ϵ_{min} and the empirical coefficients a_0 and a_1. The two model variants, with and without snow cover, are calibrated for each sub-basin and for original and corrected rainfall

input separately.

Model variants were calibrated for the two selected winter periods 2013/2014 with a pre-run loop of one year with maximum 20 iterations to equlibrate soil, interception, groundwater and river storages to the conditions present at the beginning of the actual model run. For the winter 2014/2015, for example, the modeling period covers the seven months from October 2014 until April 2015 and the pre-run loop the preceding year, October 2013 to September 2014. In total, 16 individual calibration exercises were performed.

3 Results

3.1 Precipitation gauge correction

The precipitation gauge correction algorithm detected between 5 and 20 measurement periods affected by solid precipitation (Tab.4). Those snow periods extend up to more than 20 days. In general, the higher a rain gauge is located, the more rainfall is corrected by the employed algorithm. According to the gauge correction algorithm, solid precipitation only plays a minor role at gauge stations located at low elevations of the study area, e.g. Via1 and Villacarli_Bridge_1. At Villacarli_Bridge_1 only 11 days of the total time frame considered, the correction algorithm is active. During the as cold classified months (December until March) 5.1% of rainfall measurements are affected by snow fall at this low lying station. At higher stations such as Chordal, Calvera, Las_Paules and Via2 (Tab.3) about one third of the precipitation during the cold months is affected by the correction. The amount of rainfall during those months increases of about 7% for high located rain gauges.

Table 4: Summary results of precipitation gauge correction. Given for the total time frame considered (total) and in addition for the four month December, January, February and March (cold). For each station: cumulative sum rainfall before correction [mm], the amount of rainfall added during the correction process [mm], cumulative sum of rainfall after applying the correction [mm], the increase of rainfall due to the correction [%], the total amount of rainfall affected by the correction algorithm [mm] and [%], total amount of days affected [day] and [%], the number of periods detected during solid precipitation might affect the measurement [-] and the shortest period, longest period and mean length of periods detected [day].

	Cab1	Cab2	Calvera	Chordal	Las_Pau.	Via1	Via2	Villacar.
	total|cold	total|cold	total|cold	total|cold	total|cold	total|cold	total|cold	total|cold
Cum. rain bef. [mm]	3102 | 874	2618 | 813	2721 | 721	2517 | 648	3274 | 867	2599 | 713	3570 | 963	2735 | 751
Amount added [mm]	41 | 40	42 | 37	80 | 59	43 | 40	69 | 66	15 | 15	62 | 62	10 | 10
Cum. rain aft. [mm]	3142 | 914	2660 | 850	2801 | 780	2560 | 688	3343 | 933	2614 | 728	3632 | 1025	2745 | 761
Increase rain [%]	1.3 | 4.5	1.6 | 4.6	2.9 | 8.2	1.7 | 6.2	2.1 | 7.6	0.6 | 2.1	1.7 | 6.5	0.4 | 1.3
Rain affected [mm]	162 | 158	169 |148	320 | 237	173 | 161	276 | 263	61 | 61	249 | 249	38 | 38
Rain affected [%]	5.2 | 18.1	6.5 | 18.3	11.8 | 32.9	6.9 | 24.9	8.4 | 30.3	2.4 | 8.6	7.0 | 25.9	1.4 | 5.1
Days affected [day]	46 | 45	53 | 51	82 | 75	69 | 67	75 | 72	24 | 24	73 | 73	11 | 11
Days affected [%]	3.6 | 9.3	4.2 | 10.5	6.4 | 15.5	5.4 | 13.8	5.9 | 14.9	1.9 | 5.0	5.7 | 15.1	0.9 | 2.3
Number periods [-]	8 | 7	12 | 10	17 |13	17 | 15	20 | 17	7 | 7	9 | 9	5 | 5
Short. period [day]	1 | 2	1 | 1	1 | 1	1 | 1	1 | 1	1 | 1	1 | 1	1 | 1
Mean period [day]	5.7 | 6.4	4.4 |5.1	4.8 | 5.8	4.1 | 4.8	3.8 | 4.2	3.4 | 3.4	8.1 | 8.1	2.2 | 2.2
Long. period [day]	20 | 20	18 | 18	18 |18	18 | 18	16| 16	5 | 5	22 | 22	4 |4

3.2 Relative elevation

From WASA-SNOW computed elevations range from 927-1978 m for Villacarli and 1118-2530 m for Cabecera (Fig.8). To get absolute elevations, the mean elevation of the corresponding sub-basin was added to the relative elevation of each TC. For both sub-basins, the modeled elevations cover smaller elevation ranges compared to the real topography (Tab.2). Individual toposequences cover different elevation ranges depending on length and mean elevation of the toposequence and slopes of the TCs (Fig.8). The usage of information on areal fractions of TCs within LUs and of LUs within its sub-basin allow the comparison of the elevation distribution of modeled elevations and real topographic values derived from the digital elevation model (DEM) (Fig.9). In general, pattern coincide. However, modeled results show a more uneven pattern with local peaks compared to the smooth distribution from the DEM. Furthermore, WASA-SNOW tends to underestimate areal fractions of elevations at the fringes of the elevation ranges.

3.3 Model run comparison

3.3.1 Temperature

As mean sub-basin elevation of Cabecera is greater than for Villacarli (Tab.2), the linear adjustment of temperature during interpolation is resulting in lower model input temperatures for Cabecera than for Villacarli (e.g. Fig.10e, Fig.11e). Within each sub-basin this input temperature is adjusted according to TC-elevation using a lapse-rate based approach (see section 2.1.2.4). This adjustment is resulting in intra-sub-basin temperature differences according to elevation of 8.47 (6.31) °C in Cabecera (Villacarli) between the highest and lowest located TC (e.g. Fig.10e, Fig.11e). During winter months input temperatures generally fluctuate around 0 °C. The lapse-rate based approach is adjusting temperatures in the highest TCs to be mostly below the freezing point during winter months. Particularly cold temperatures are calculated for the high mountain peaks of Cabecera represented by five TCs of LU 79, having the TC indexes 123 to 127 in Fig.3b. However, temperatures at the lower located TC seldom fall below the freezing point. In the area of interest, there generally is a constant switch between temperatures favoring

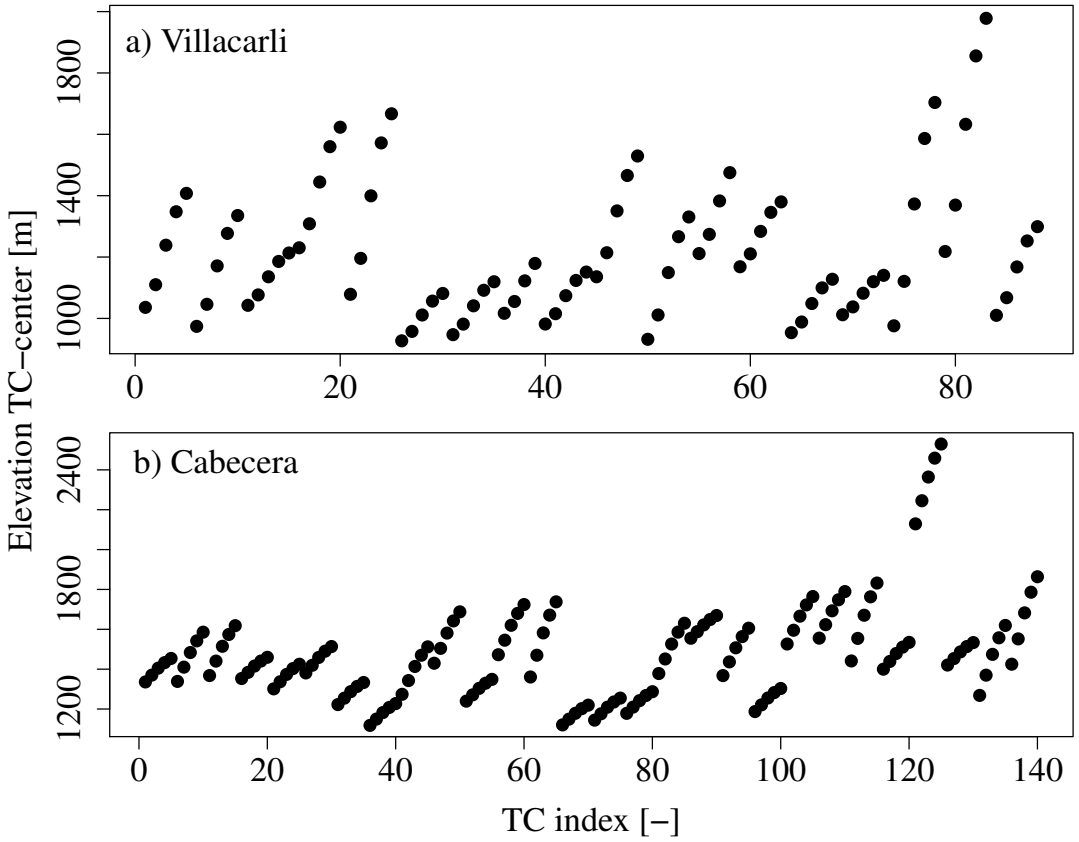

Figure 8: Elevations of TC-centers for the two sub-basins a) Villacarli and b) Cabecera

snow accumulation and favoring snow melt during the course of a winter. In addition to this temporal dynamics, spatial differences according to elevation caused by different temperatures are common. Precipitation can be considered solid at higher elevation, whereas being liquid in the lowlands. Snow cover dynamics of TCs vary according to its elevation.

In the following, those variations are described in more detail comparing SWE of TC 508, located in the Cabecera sub-basin at a relative elevation of +179 m (1682 m a.s.l.) (Fig.15a), with the sub-basin mean (Fig.12a). A continuous snow cover is present at TC 508 from mid January until the beginning of March. Snow contributing to the mean sub-basin SWE (Fig.12a) before and after this period is accumulated at higher TCs in the sub-basin. The intermediate melt events at

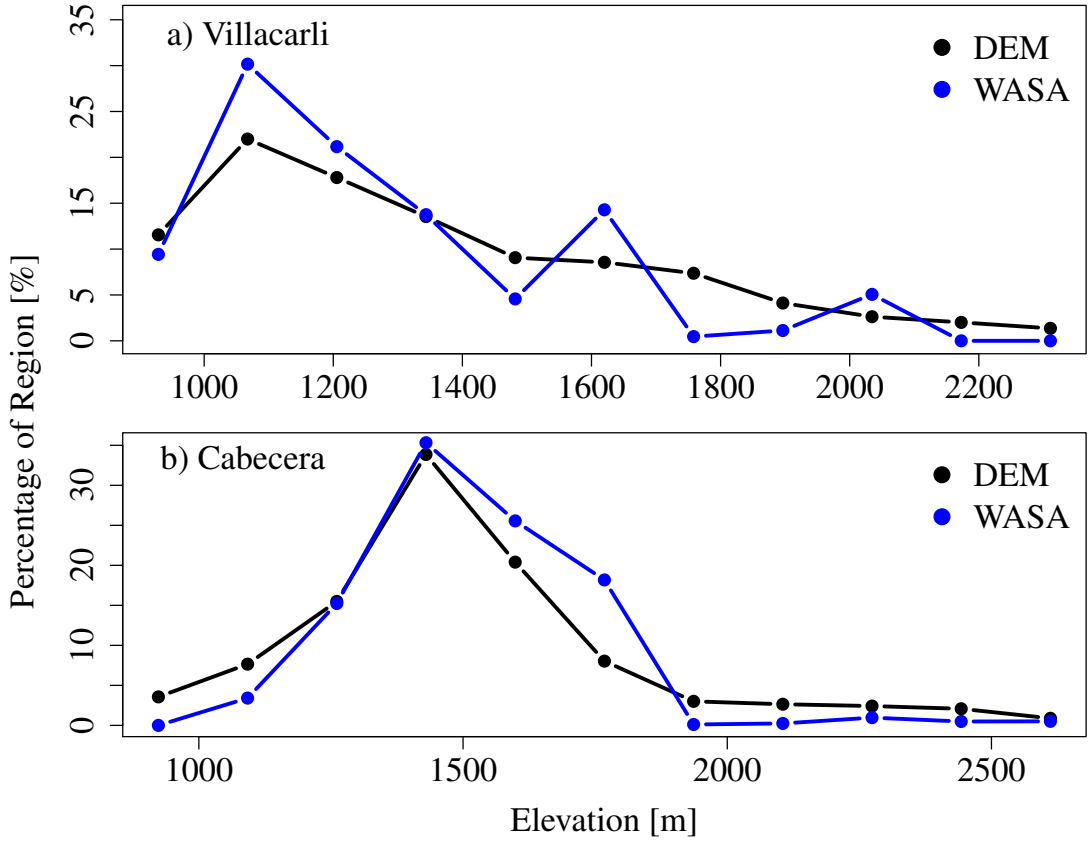

Figure 9: Elevation distribution of sub-basins investigated: a) Villacarli and b) Cabecera; black line represents values attained from digital elevation model (DEM), blue line: WASA-SNOW elevations

the end of January and in the second half of February present in the sub-basin during this period occur at lower TCs. Only little snow is melting at the end of January at TC 508 before temperatures decrease again (Fig.15d). It should be noted that temperatures modified according to elevation and presented in panel e) of the model comparison result plots is in addition adjusted for intermediate time steps assuming a sinusoidal diurnal temperature variation (see section 2.1.2.6).

3.3.2 Precipitation

During the two more closely investigated winter periods, precipitation characteristics differ considerably. The winter period 14/15 is relatively dry with particularly

few precipitation form December until February (Fig.12a,g). Substantially more rain is falling during the winter period 2013/2014. For the Cabecera sub-basin rain accumulates to more than 400 mm between December and April (Fig.10g), compared to less than 200 mm for the same months during winter 2014/2015 (Fig.12g). During the winter period 14/15 the gauge correction algorithm only detects one bigger event in the second half of March. Modifications for this event reach magnitudes of up to 10 (4) mm for Cabecera (Villacarli) for this event (Fig.12g, Fig.13d). During the winter period 13/14 precipitation of a period of more than 20 days at the turn of the month from January to February is redistributed and corrected by the gauge correction algorithm. Modifications reach magnitudes up to 25 (15) mm for Cabecera (Villacarli). In general, first solid precipitation tends to fall in the month of November. During this month temperatures start to fall below the freezing point at the highest elevations of the area (Fig.12e). With rising temperatures above the freezing point no later than April, snow fall becomes an exceptional event.

3.3.3 Discharge

3.3.3.1 Villacarli

For the winter period 13/14 no model variant was capable of simulating the discharge dynamics measured at the outlet of the sub-basin (Fig.11c,d). During model calibration for this period parameter sets with maximum possible hydraulic conductivity during the infiltration processes, bedrock thickness and groundwater delay and minimum possible hydraulic conductivity within the bedrock are returned as optimum parameter sets (Fig.18). Consequently, almost all water reaching the surface immediately infiltrates into the soil, percolates very snow through a thick bedrock layer before being added to the river discharge from the groundwater storage with maximum delay. A smooth decreasing and descending discharge is the result.

Model results indicate that water volume available during simulation generally is higher than the measured values. A WASA model run with inactive snow module in Villacarli for the winter periods 13/14 with the parameter set of Cabecera for this periods further hints at this mismatch of water volume between simulation and

measurement (Fig.14b). Using the Cabecera parameter set, the general dynamics of the discharge are simulated better. However, the RMSE attained with the exchanged parameter set is higher than the value achieved during model calibration for Villacarli. The calibration routine worked correctly and returned the parameter set with lowest objective function. Snow cover calculated by the snow module is dynamic and several events of accumulation and melt can be distinguished. However, due to the general difficulties of the model during this period, results are only of limited informational value.

Model performance for the winter 14/15 is substantially better. All model variants are able to capture the discharge dynamics for this period. However, during the dry months at the beginning of the year 2015, again more water seems to be available in the model than measured at the outlet. In the course of this dry period, measured discharge levels off to values of only some tens of liters and even short periods of no discharge at all are recorded. Also the few rain events occurring during this period almost have no effect on the measured discharge.

During model runs with active snow routine, first snow is accumulated at the beginning of November (Fig.13a,b). For the greatest part of the sub-basin, snow cover is present only periodically. Snow dynamics are characterized by several phases of accumulation and melt. The sub-basin mean SWE reaches maximum values of around 2 cm. This snow is concentrated at higher located TCs. No model improvement due to activation of the snow module is visible. The usage of gauge corrected rainfall input data instead of original data leads to the selection of a different best parameters set during model calibration and different model behavior also during periods not directly affected by the gauge correction. Main difference is a higher threshold temperature T_{crit} (3.95 °C) for solid precipitation using gauge corrected rainfall input compared to the calibration run with original rainfall input data (2.96 °C) is selected. This high threshold temperature is causing more rain to fall as solid precipitation and accumulate (Fig.13b). For both model variants, T_{crit} takes unusual high values, indicating the model trying to favor the accumulation of snow.

3.3.3.2 Cabecera

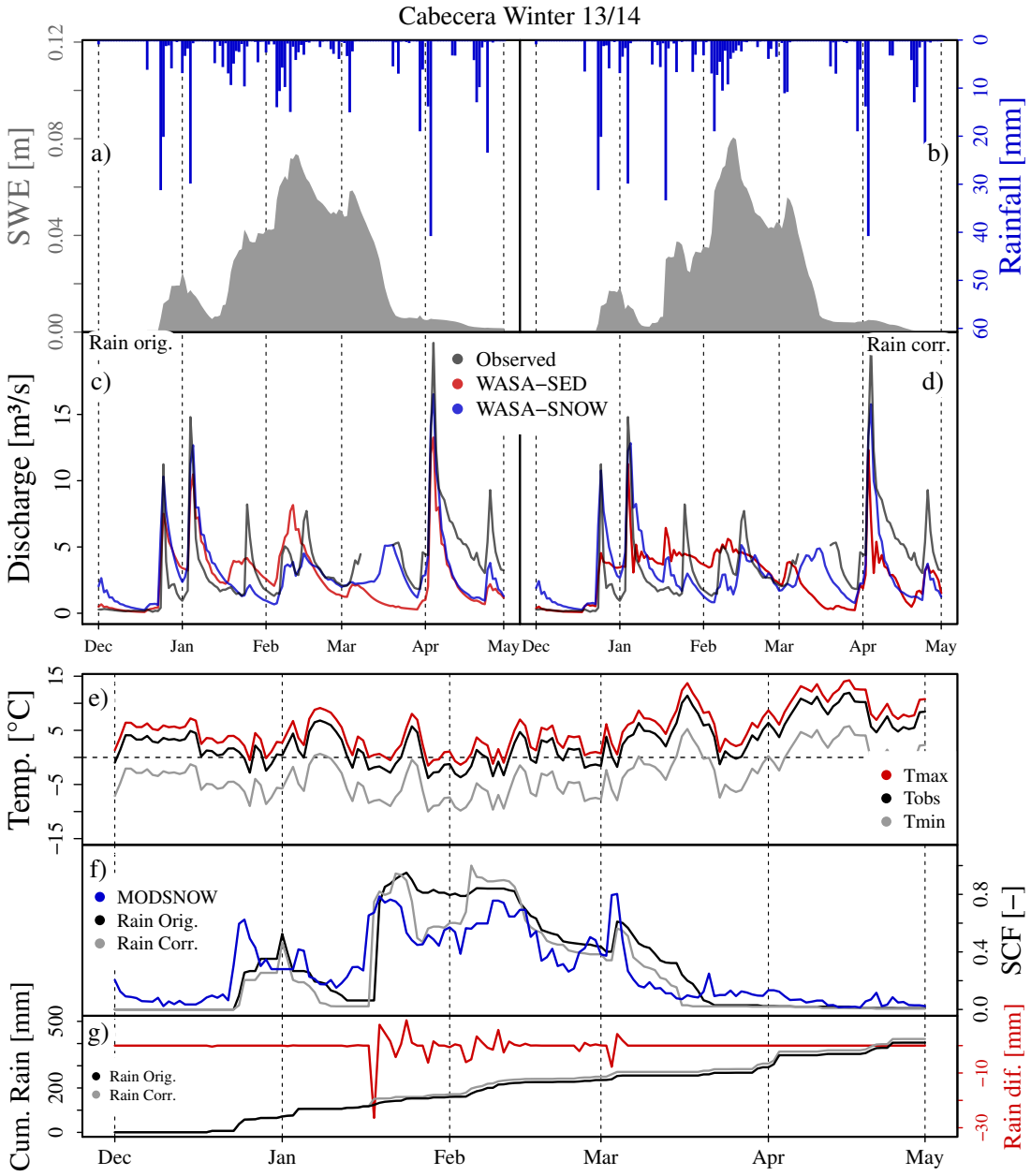

Figure 10: Model results: Snow water equivalent (SWE) and comparison of discharge observed and simulated with (WASA-SNOW) and without (WASA-SED) snow routine for original rainfall input (a and c) and corrected rainfall input (b and d); Temperature input (Tobs) and Tmax and Tmin temperature (highest and lowest TC) attained through lapse-rate based modification (e); Comparison of modeled snow cover fraction and MODSNOW data (f); Difference of orig. and corrected rainfall signal and cumulative rainfall (g).

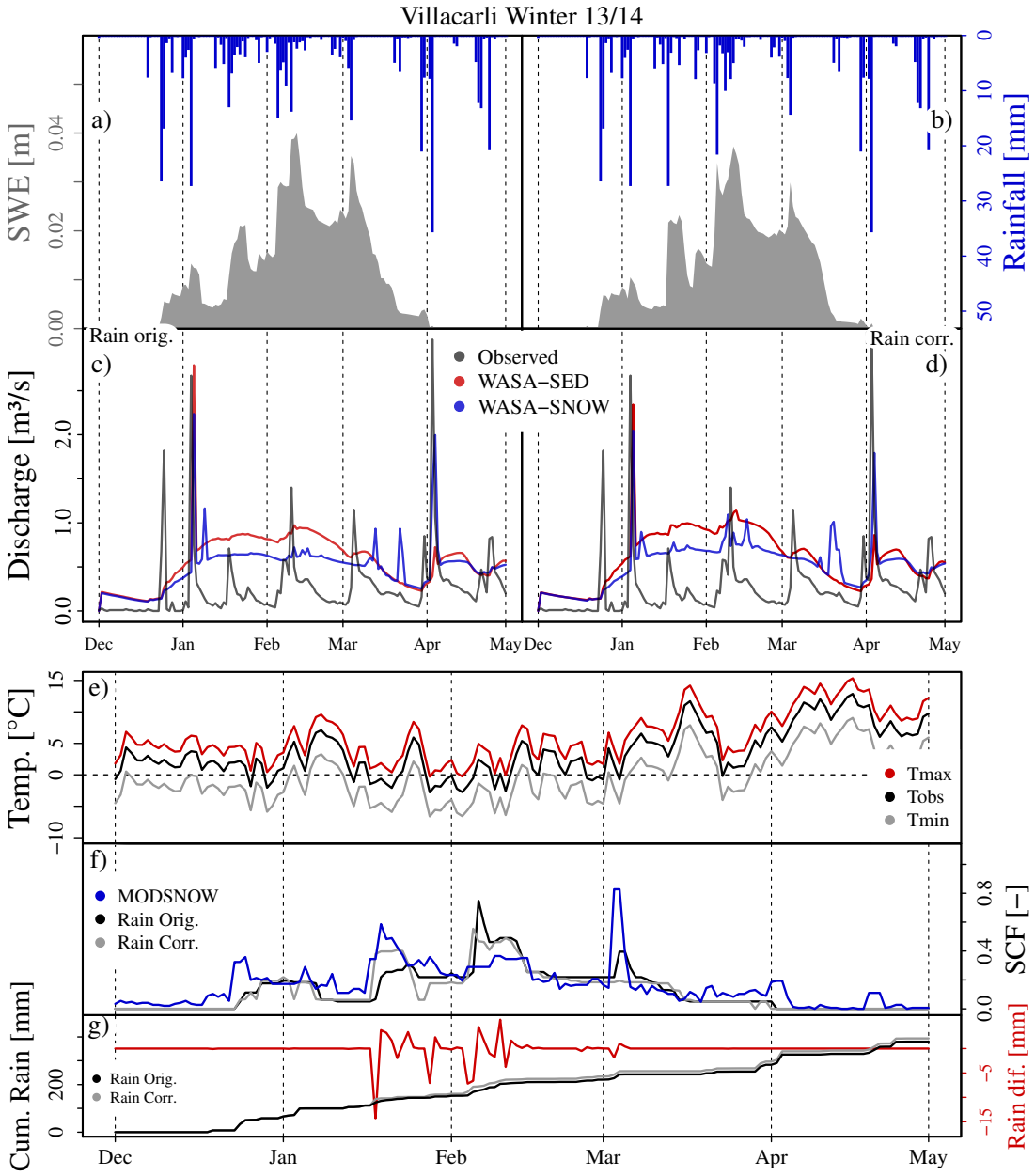

Figure 11: Model results: Snow water equivalent (SWE) and comparison of discharge observed and simulated with (WASA-SNOW) and without (WASA-SED) snow routine for original rainfall input (a and c) and corrected rainfall input (b and d); Temperature input (Tobs) and Tmax and Tmin temperature (highest and lowest TC) attained through lapse-rate based modification (e); Comparison of modeled snow cover fraction and MODSNOW data (f); Difference of orig. and corrected rainfall signal and cumulative rainfall (g).

For the winter period 13/14, WASA with inactive snow module is able to capture discharge dynamics when run with original rainfall data (Fig.10c). At the attempt to calibrate WASA-SED with gauge corrected rainfall input data, the model reaches its limits to simulate the measured discharge (Fig.10d). The gauge correction algorithm is shifting precipitation towards an event in mid-January. This change in the rainfall input signal is causing the calibration routine to select a parameter set with a thicker bedrock layer and higher groundwater delay compared to the parameter set attained during calibration with original rainfall input data. A damping of the discharge signal is the result. Usage of the parameter set attained from calibration with the original rainfall input during a model run with corrected data hints at the high magnitude of the new rainfall event the calibration routine tries to dampen, as no corresponding response in the discharge measurements is recorded (Fig.14a).

During the model run with WASA-SNOW, this new rainfall event is mainly accumulated in the snow cover and contributes to the stream flow during snow melt in mid-March (Fig.10b,d). In general, dynamics of the snow cover with its different phases of accumulation and melt help WASA improve model performance for this period. The two discharge peaks recorded in February can be distinguished and snow melt during March is providing necessary input to the river network to simulate measured values. Snow accumulated at the highest TCs of the sub-basin is not fully melted before mid-April.

Also during simulations of the winter period 14/15, the snow routine helps to improve model performance (Fig.12c,d). WASA-SNOW is storing precipitation falling during January and February in the snow cover and returns this temporarily stored water via snow melt at the beginning of March. WASA-SED not having this temporal water storage overestimates discharges during the rainfall events in January and February and is not able to simulate river flow at at the beginning of March. The usage of corrected rainfall input data improves model performance.

3.3.4 Snow cover fraction

Due to the difficulties of model applications in the Villacarli sub-basin, comparisons of modeled and satellite-derived snow cover data for Cabecera contain higher

informative value. Generally, observed and simulated snow cover areas coincide (Fig.10f,12f). Snow events simulated in the model are visible in satellite-derived snow data. Observed snow cover areas are characterized by stronger short term changes. Furthermore, after a snow event, the area of snow cover tends to stay constant for some time in the model, whereas the observed area starts to decrease shortly after the event.

3.3.5 Snow cover dynamics

The functioning of the snow routine as precipitation pre-processing tool is presented in Fig.15a. In this figure not the difference between original and corrected rainfall input data, but the the differences between rainfall signal that enters and leaves the snow routine are displayed. Positive values indicates an accumulation of rainfall input in the snow cover. Negative values represent water input caused by melt of snow, where originally no rainfall input was present.

A positive R_{netS} and energy provided by R_{sens} are responsible for energy input into the snow cover (Fig.15b). R_{netS} slowly but steadily increases as days get longer and insolation increases. R_{sens} is proportional to the temperature gradient between atmosphere and snow surface. A positive gradient leads to energy influx by sensible heat for the time period investigated (Fig.15b,d). More long-wave radiation tends to be emitted from the snow cover than absorbed, leading to a negative R_{netL}. The rainfall event end of January is classified as solid according to T_{crit} and is accumulated in the snow cover. Even though, energy is added as temperatures are above the freezing point. This added energy is sufficient for the radiation balance to become positive. This increases SEC enough to cause a part of the present snow cover to melt (Fig.15b,c).

The sublimation mass flux increases with an increasing vapor pressure gradient between snow surface and air. Highest sublimation rates are simulated when the temperature difference between snow surface and atmosphere are low and can reach values up to more than 0.4 mm/day. During phases of particularly low snow temperatures compared to atmospheric temperatures, the saturation vapor pressure at the snow cover is too low to give rise to mass and energy due to sublimation. The sublimation of in total 7.26 mm is causing the energy flux due

to sublimation displayed in Fig.15b. The phase change of solid to liquid consumes surplus energy available, which is removed from the snow cover by outflow of meltwater.

4 Discussion

4.1 Precipitation gauge correction

The approach proved to be able to dynamically detect measurement periods possibly affected by solid precipitation. The usage of a degree day melt model to determine the length of periods affected by snow fall and melt enables flexible period length detection. However, a thorough validation of the method still is pending. Parameters for the degree day factor, the threshold temperature for solid precipitation and for increased under-catch of solid precipitation are just simple assumptions and do not base on statistical analysis of local data. Further limitation of the approach are the negligence of other gauge measurement errors and the usage of just one base station. The usage of satellite-derived information on days with snow cover or the evaluation of photographic or video material from measurement sites could represent a first step in evaluating the presented approach.

Model results indicate that the hypothesis that snow gauge measurement devices itself function as precipitation pre-processing tool by storing and melting snow in its collector device, making the usage of a snow module in WASA obsolete, can not be confirmed. Assuming the correction algorithm being able to reconstruct the true liquid precipitation signal, WASA-SED should perform better with original rainfall input data than with the corrected signal. A WASA-SED run with original data should perform similar to WASA-SNOW. This is not the case.

As all rainfall measurement sites are located below 1600 m a.s.l., mainly the lower elevations of the sub-basins, not as much being affected by snow processes, which are getting more and more prominent at higher elevations, are sampled. The measurement network might not record a solid precipitation signal representative for the whole area. Very different conditions in the collector bucket compared

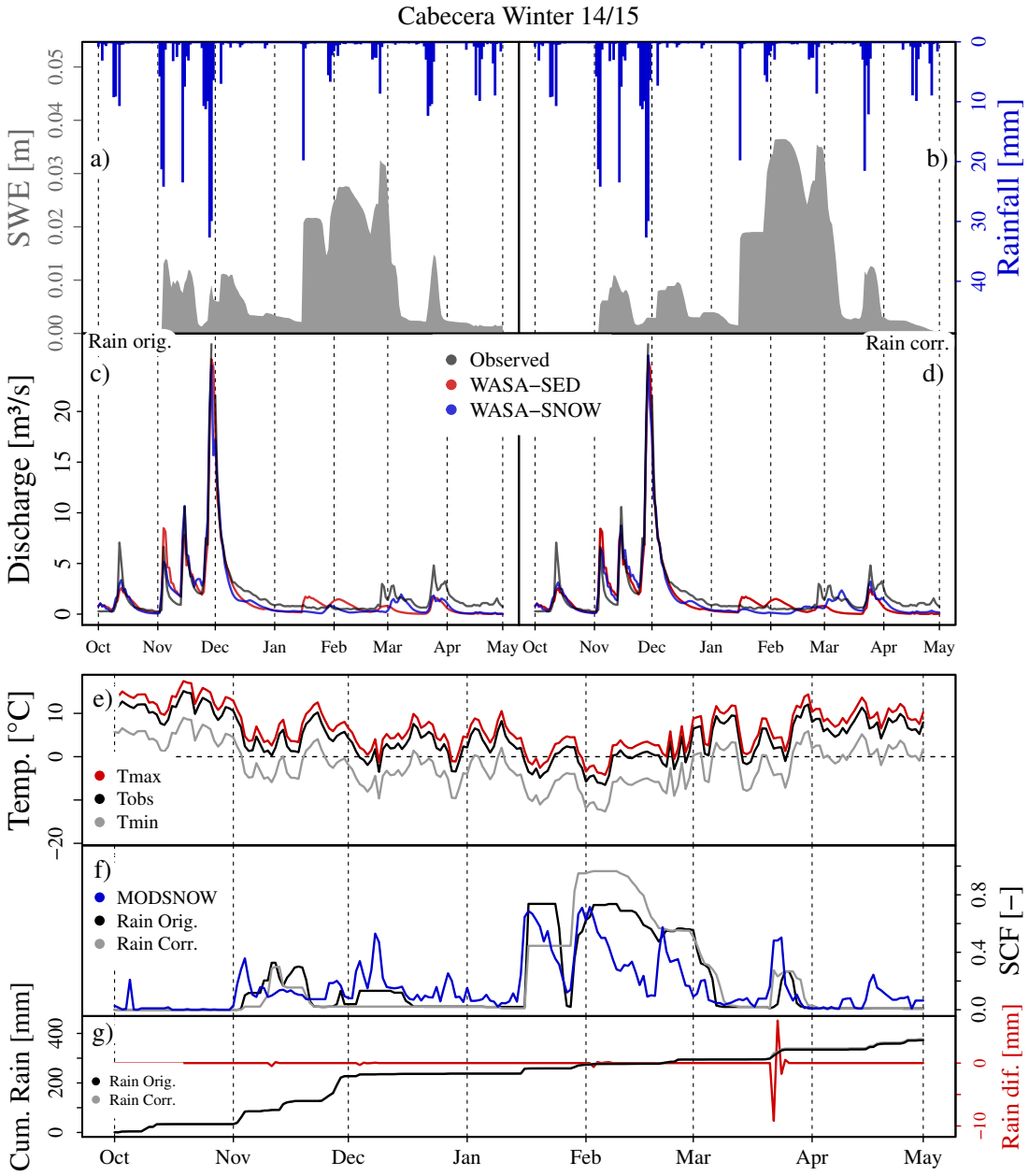

Figure 12: Model results: Snow water equivalent (SWE) and comparison of discharge observed and simulated with (WASA-SNOW) and without (WASA-SED) snow routine for original rainfall input (a and c) and corrected rainfall input (b and d); Temperature input (Tobs) and Tmax and Tmin temperature (highest and lowest TC) attained through lapse-rate based modification (e); Comparison of modeled snow cover fraction and MODSNOW data (f); Difference of orig. and corrected rainfall signal and cumulative rainfall (g).

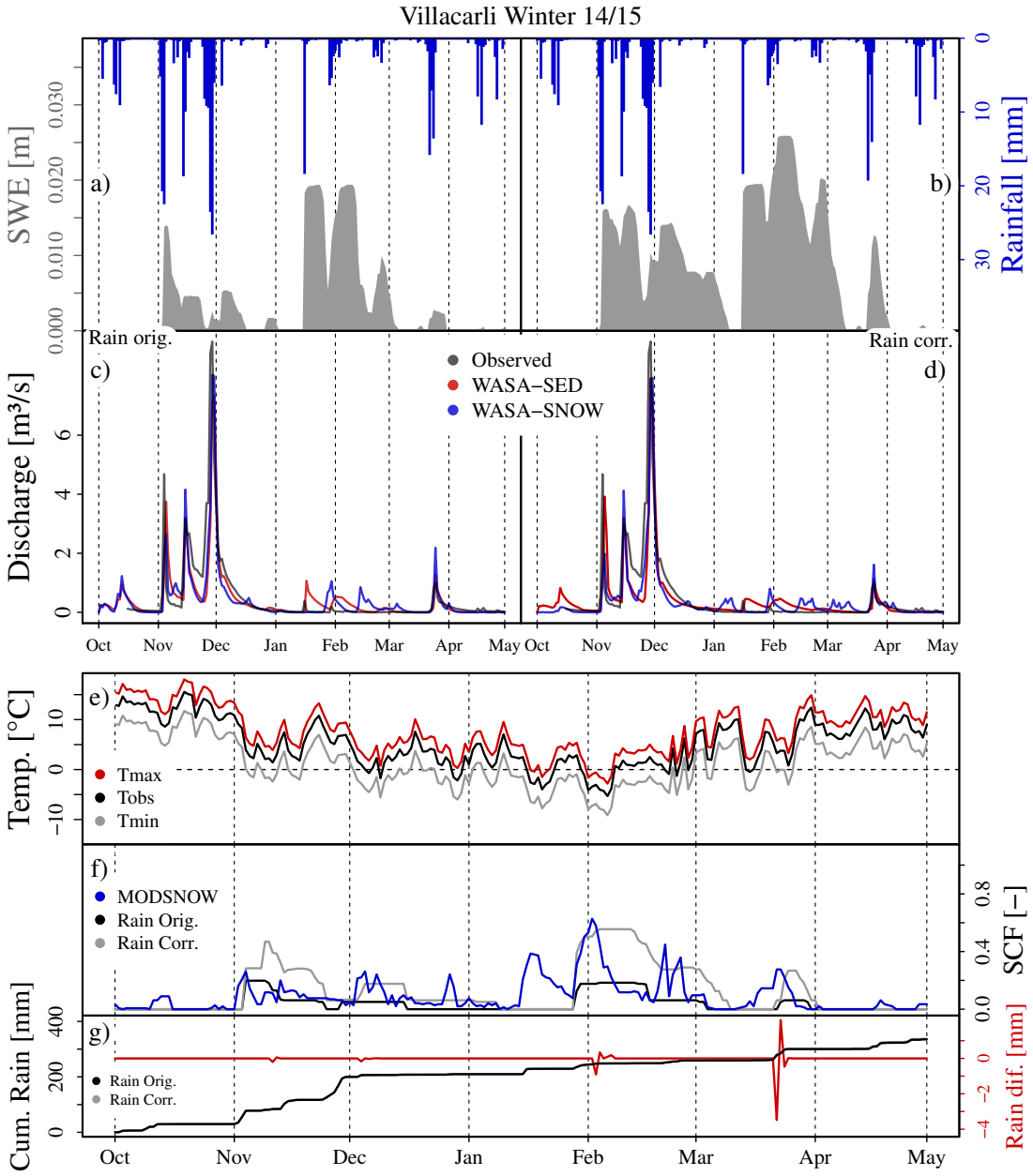

Figure 13: Model results: Snow water equivalent (SWE) and comparison of discharge observed and simulated with (WASA-SNOW) and without (WASA-SED) snow routine for original rainfall input (a and c) and corrected rainfall input (b and d); Temperature input (Tobs) and Tmax and Tmin temperature (highest and lowest TC) attained through lapse-rate based modification (e); Comparison of modeled snow cover fraction and MODSNOW data (f); Difference of orig. and corrected rainfall signal and cumulative rainfall (g).

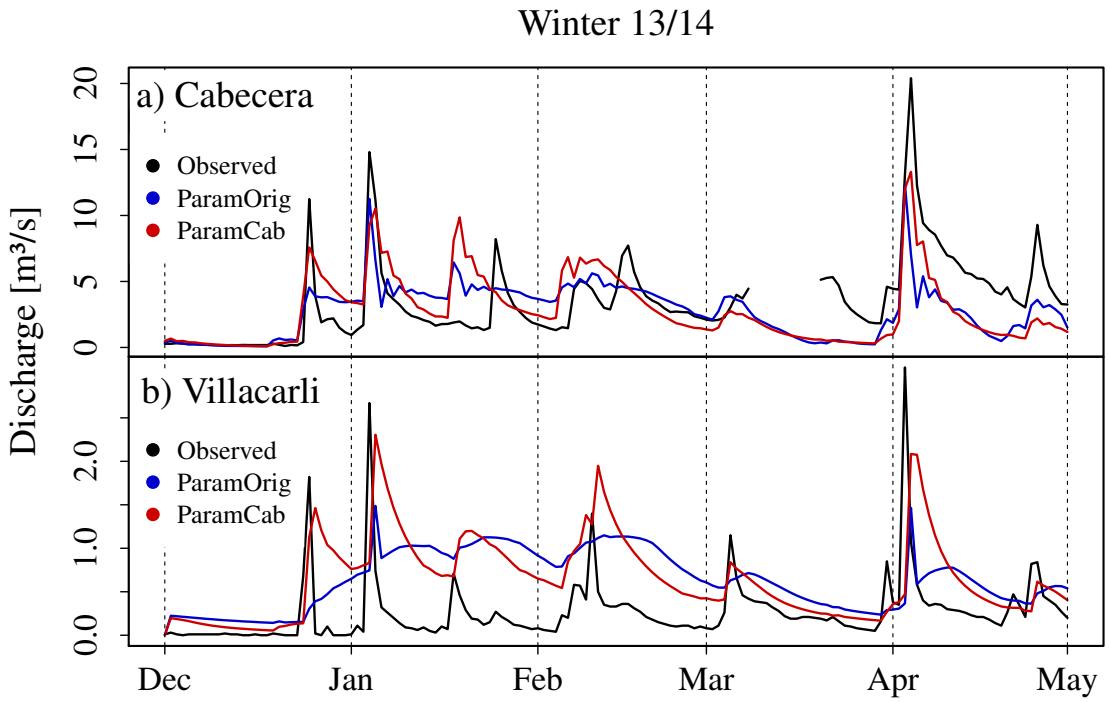

Figure 14: WASA model runs with exchange parameter sets: a) Cabecera winter 2013/2014 rain corrected run with originally attained parameters set (ParamOrig) and parameter set from calibration run with uncorrected rain data (ParamCab); b) Villacarli winter 2013/2014 uncorrected rainfall run with originally attained parameter set (ParamOrig) and parameter set attained from calibration run for Cabecera sub-basin for similar rainfall input and time frame (ParamCab).

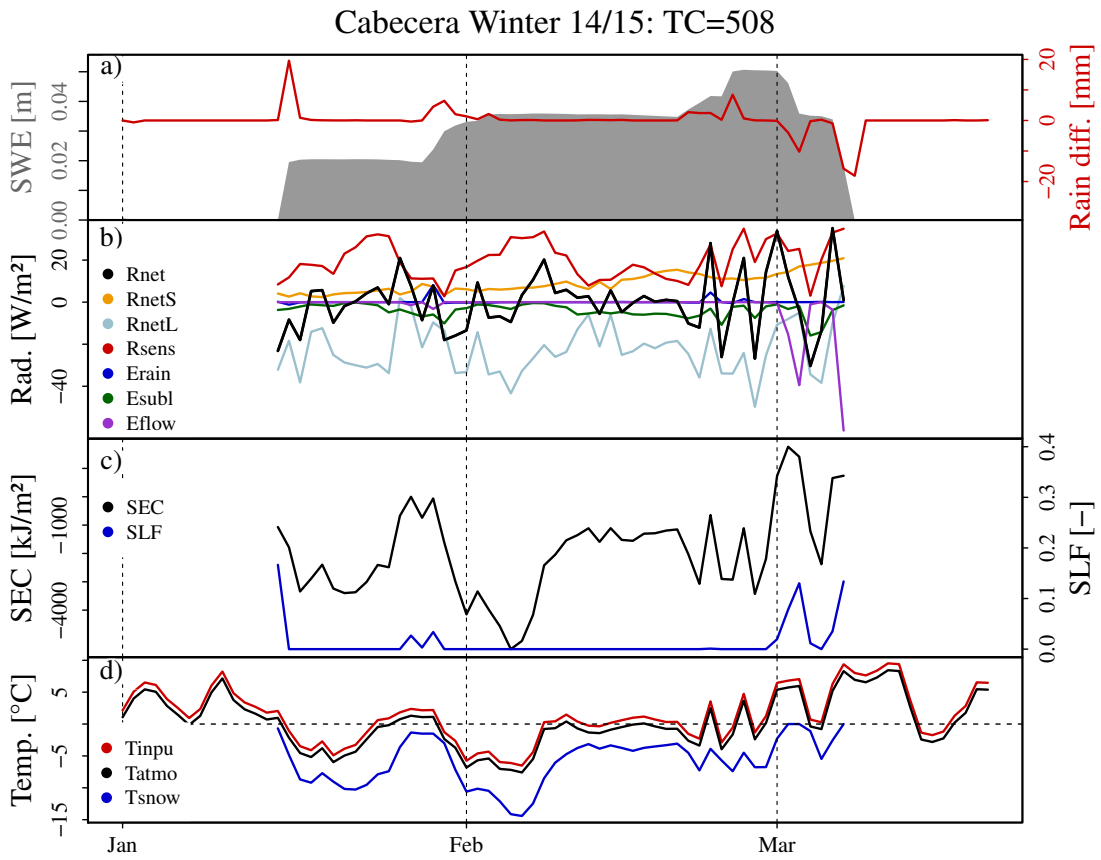

Figure 15: Snow cover dynamics Cabecera winter 2014/2015, TC 508: a) Snow water equivalent and precipitation pre-processing by the snow module displayed as differences between rain input and output of the snow module; b) Snow cover energy balance with total net radiation R_{net}, short-wave radiation balance R_{netS}, long-wave radiation balance R_{netL}, sensible heat flux R_{sens} and energy fluxes due to mass fluxes of precipitation E_{rain}, sublimation E_{subl} and meltwater E_{flow}; c) Snow energy content SEC and snow liquid fraction SLF of the snow cover; d) Model input temperature on sub-basin scale T_{inpu}, atmospheric temperature of TC T_{atmo} attained by lapse-rate based modification of T_{inpu} and snow surface temperature T_{snow}.

to the surroundings, might impede similar snow accumulation and melt behavior. Also shortcomings of the correction algorithm itself can not be ruled out.

4.2 Elevation dependent meteo-driver adjustment

The comparison of modeled elevations with real topographic values and the examination of individual TC-elevations confirm the method used to provide realistic elevations for TCs. However, the method reaches its limits when it comes to capture very low and high elevations. It can not represent the whole elevation range present in the study area. Only few data points, the number of TCs, are available to represent the whole area. Certain elevations get over- or underrepresented by individual TC-elevation values (Fig.9). Representative toposequences used in this study initially were derived for the whole Isábena catchment. Applying the LUMP algorithm with elevation as characteristic to derive LUs could improve the elevation representation of the sub-basins investigated.

The lapse-rate based temperature adjustment using the relative TC-elevation enables to address intra-sub-basin temperature differences according to elevation. Due to the high elevation range covered, the height-dependent adjustment of temperature represents a crucial step in simulating spatial variability of snow dynamics in the area. The lapse-rate used to adjust temperature according to elevation is assumed constant. A look a the temporal evolution of the temperature lapse-rate in the study area revels that this is hardly the case (Fig.16). Temperature lapse-rate is a very dynamic parameter and even situations of inversion occur, which the model for now is not able to capture. Further analysis of sensitivity of the model towards those modifications is needed. A first step could be the comparison of model runs with and without height-modification of temperature adjusting the logical the parameter do_alt_cor in the snow control file. In addition to investigate the effect of temperature adjustments, testing the applicability of radiation modification for aspect and slope implemented still is pending. The correction of incoming radiation for aspect and slope is believed to be an important feature of snow simulations. Snow cover dynamics can differ considerably depending on exposure of slopes. The newly available information on relative elevation and aspect are highly valuable and the task of future work might be to assess, whether the

usage of this information can help to improve simulations of other hydrological processes. A general adjustment of temperature and rainfall input data according to elevation and radiation according to aspect and slope might improve overall model performance by addressing for the spatial variability caused by the topography of the study area.

4.3 Model run comparison

4.3.1 Villacarli

In general, WASA is having difficulties simulating river discharge measured at the outlet of the Villacarli sub-basin. This can have several reasons. First of all, the WASA model itself is not be able to simulate processes in the area. Some important hydrological features might not be included into the model yet. Furthermore, WASA is operating at its limits regarding areal extend of the sub-basin. With only 38 km^2 the Villacarli sub-basin is situated at the lower limit of the for meso-scale applications developed WASA model. LUs for the sub-basin where derived during spatial disaggregation of the whole Isábena catchment. Applying the LUMP-algorithm for the area explicitly might improve the representation of the topography. Also the temporal resolution selected for the model runs might be to low. Hourly instead of daily resolution data possibly helped capturing the fast rainfall-runoff reaction present within the sub-basin.

Secondly, shortcomings of the calibration routine could be reason of the poor model performance in the Villacarli sub-basin. The DDS algorithm used during calibration proved to be a powerful tool. Best performing parameter sets were found easily during the calibration process. However, what has to be questioned is the choice of objective function. The usage of a single-objective approach based on RMSE in some cases lead to the selection of unrealistic parameter sets causing all discharge dynamics to be lost and making the model results useless for further investigations. Other single- and multi-objective calibration models are available and their applicability has to be assessed in further investigations. Multi-objective calibration might represent a promising approach (Tian2016). Multi-objective model calibrations usually base either on multi-variable measurements, multi-site measurements or multi-response modes (Madsen2003, Tain2016, Madsen2000). The

inclusion of the satellite-derived snow cover data into the calibration could represent the first step in improving model calibration of WASA-SNOW model applications.

Thirdly, the possibility of erroneous discharge data can not be excluded. The measurement site is characterized by very challenging measurement conditions. The bridge at which measurement devices are installed is located in a wide gravel bed. The river bed is very dynamic and the river profile under the bridge is subject to constant changes. Discharge values are determined using stage measurements and invariant rating curves estimated with Baratin (Francke et al., 2017a). The unsteady site conditions might cause under- and overestimation of discharge during certain periods of the measurement time. Very low runoff coefficient for large periods might indicate that portions of water leaving the sub-basin are not recorded (Fig.17). Parts possibly leave the sub-basin as hyporrheic discharge through the vast loose gravel layer at the bottom of the valley. In comparison to Villacarli, discharge at the outlet of the Cabecera sub-basin is measured at a solid weir based on bedrock.

4.3.2 Cabecera

The model proved to be able to simulated discharge measured at the outlet of the sub-basin. Activation of the snow routine and the temporal build up of a snow cover further improves simulations. The snow cover in the area is very dynamic and several events of accumulation and melt occur. Difficulties of WASA-SED simulating the winter period 2013/2014 with corrected precipitation input data can have two reasons. First, the correction algorithm was able to reconstruct the true liquid precipitation signal and the model is not able to simulate discharge without snow cover dynamics. Secondly, the reconstructed liquid rain signal is not correct. The snow period detected by the correction algorithm is quiet long causing high amounts of rainfall being redistributed according to the base station signal. Too much rain might have been attributed to the event in the middle of January.

4.4 Snow cover

Satellite-derived snow cover data is used to validate internal model consistency. The comparison of modeled and observed values proves internal processes of the model to be valid. The general patterns of the temporal evolution of observed and simulated snow cover fractions coincide. The resolution of the snow fraction output of the model still is limited. An individual TC for now only is considered as fully covered by snow or not covered by snow at all according the threshold of SWE determined. The addition of a snow depletion curve to address for spatial variability of the snow cover within a TC represents a good opportunity to further improve snow fraction calculations of the WASA snow routine. A corresponding function called snowDepl located in snow_compute already exists and could provide the necessary frame for this task. The tendency of snow cover to decrease faster directly after the event in observations might be due to the lack of the representation of spatial variability of snow cover within TCs. It also might indicate snow to melt more steadily and not as abrupt as often simulated by the snow routine. Stronger short term fluctuations in the observed data might hint at snow events in higher elevation not captured by the model.

5 Conclusion

A physically-based snow routine is available for future WASA-SED model applications. A first test application in the two headwater catchments of the Isábena river shows the routine being able to capture snow dynamics. The activation of the snow routine helps the WASA model to simulate measured discharge during from snow affected periods. The physical basis of the snow module proved to be capable of representing complex snow dynamics. The Villacarli sub-basin turned out to represent a challenging area for WASA model applications. As long as underlying causes are not fully understood, caution has to be exercised in future applications in this area.

Comparison of different model variants indicates that the precipitation measurement network is not recording a solid precipitation signal representative for the region. Further investigations are necessary to better understand rain gauge

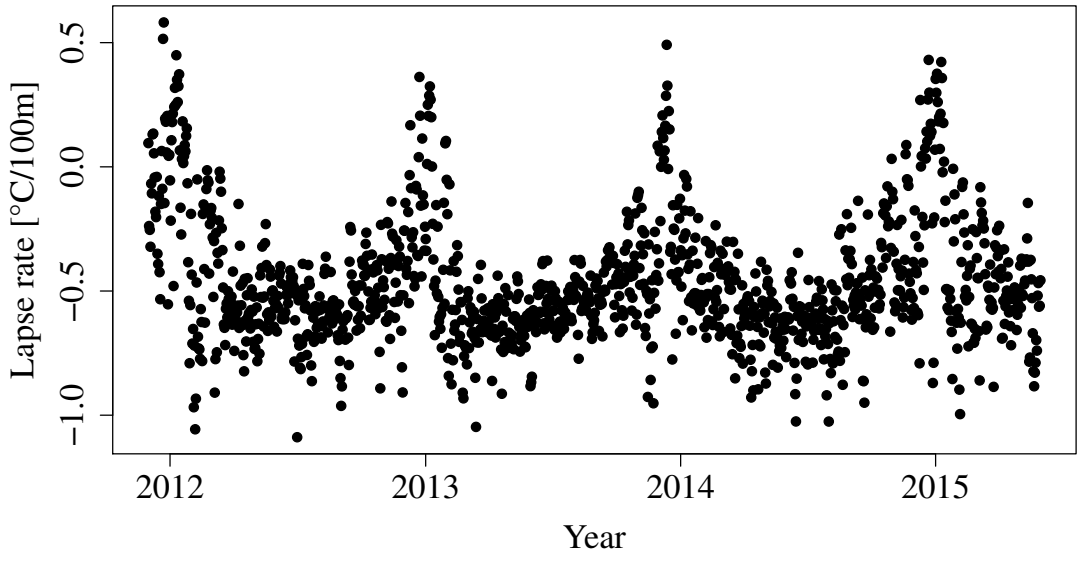

Figure 16: Temporal evolution of temperature lapse rates computed using available temperature time series from Campo, Cerler, Las_Paules and Villacarli_Bridge

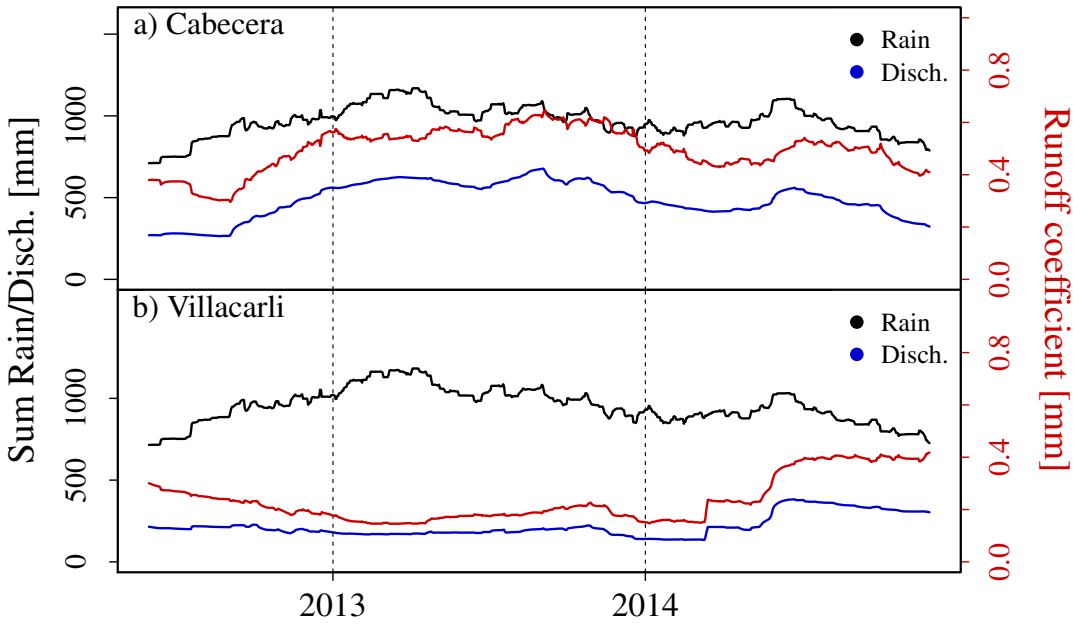

Figure 17: Runoff coefficients for Cabecera and Villacarli sub-basins attained from 1-year running sum values of discharge and precipitation

catch behavior of installed measurement devices and to validate the rain gauge correction algorithm applied in the framework of this study. Information on snow cover derived from satellite images could represent a first step in further improving the employed algorithm and parameters.

The work conducted in the framework of this master thesis only represents a first step in the process of implementing and evaluating a physically-based WASA-SED snow routine. Further improvements and testing are necessary. Future tasks include the implementation of a snow depletion curve into the snow routine, the conduction of model runs in hourly resolution and applications in areas outside the Isábena river catchment. Within this study only six selected snow parameters have been calibrated. Further detailed investigations on the sensitivity of snow parameter might provide useful information on which and how many snow parameter to calibrate in WASA application with activated snow routine. Furthermore, newly available information on elevation and aspect can also be used in model compartments outside the snow routine. The integration of snow cover data into

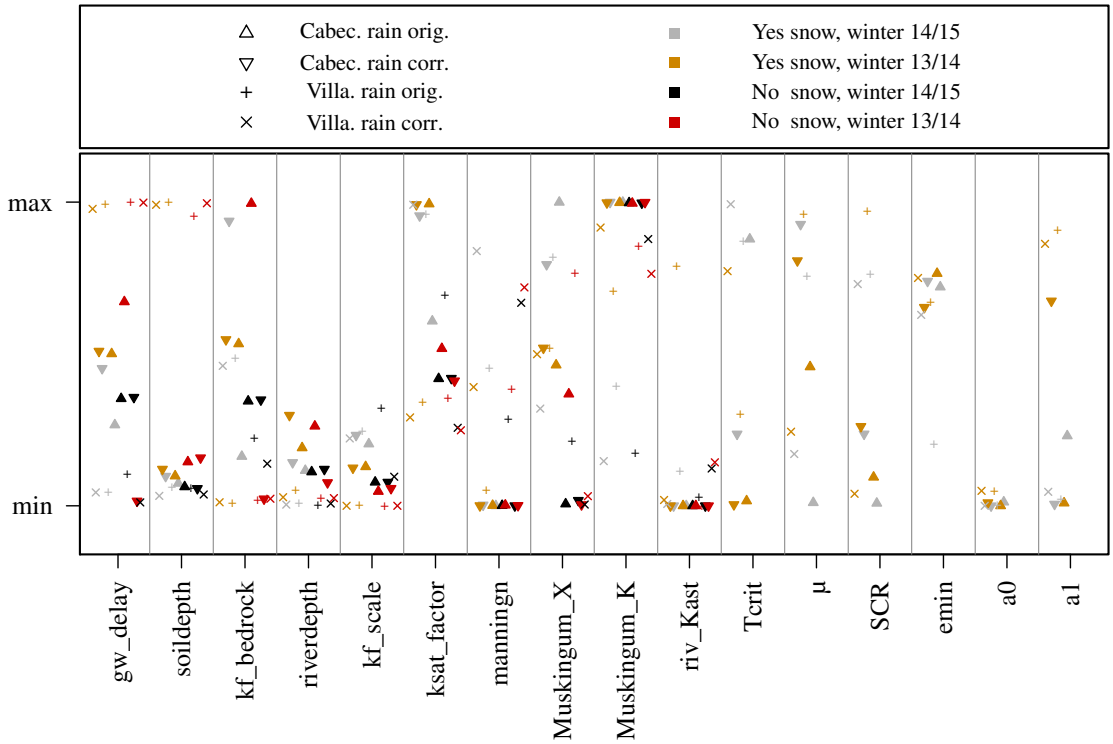

Figure 18: Comparison of 16 parameter sets attained by calibration. Displayed is the relative position of parameter values within the search range.

the calibration process represents another interesting task for future research. The information on the spatial distribution of snow in the study area, also available via the MODSNOW-tool, could prove to be useful in evaluating model applications in mountainous catchments and the influence of aspect on snow processes.

Statutory declaration

I declare that I have developed and written the enclosed Master Thesis completely by myself, and have not used sources or means without declaration in the text. Any thoughts from others or literal quotations are clearly marked. The Master Thesis was not used in the same or in a similar version to achieve an academic grading or is being published elsewhere.

Location, Date	Erwin Rottler

References

Allen, R. G., Trezza, R., and Tasumi, M. (2006). Analytical integrated functions for daily solar radiation on slopes. *Agricultural and Forest Meteorology*, 139:55–73.

Chu, J., Peng, Y., Ding, W., and Li, Y. (2015). A heuristic dynamically dimensioned search with sensitivity information (HDDS-S) and application to river basin management. *Water*, 7(5):2214–2238.

Duethmann, D., Bolch, T., Farinotti, D., Kriegel, D., Vorogushyn, S., Merz, B., Pieczonka, T., Jiang, T., Su, B., and Güntner, A. (2015). Attribution of streamflow trends in snow-and glacier melt dominated catchments of the Tarim River, Central Asia. *Water Resources Research*, 51:4727–4750.

Duethmann, D., Menz, C., Jiang, T., and Vorogushyn, S. (2016). Projections for headwater catchments of the Tarim River reveal glacier retreat and decreasing surface water availability but uncertainties are large. *Environmental Research Letters*, 11(5):054024.

Duethmann, D., Peters, J., Blume, T., Vorogushyn, S., and Güntner, A. (2014). The value of satellite-derived snow cover images for calibrating a hydrological model in snow-dominated catchments in Central Asia. *Water Resources Research*, 50(3):2002–2021.

Duethmann, D., Zimmer, J., Gafurov, A., Güntner, A., Kriegel, D., Merz, B., and Vorogushyn, S. (2013). Evaluation of areal precipitation estimates based on downscaled reanalysis and station data by hydrological modelling. *Hydrology and Earth System Sciences*, 17(7):2415–2434.

Duffie, J. A. and Beckman, W. A. (1980). *Solar engineering of thermal processes*. John Wiley and Sons, New York, NY.

Dyck, S. and Peschke, G. (1995). Grundlagen der Hydrologie. Verlag für Bauwesen, Berlin.

Efstratiadis, A. and Koutsoyiannis, D. (2010). One decade of multi-objective calibration approaches in hydrological modelling: a review. *Hydrological Sciences Journal*, 55(1):58–78.

Finger, D., Vis, M., Huss, M., and Seibert, J. (2015). The value of multiple data set calibration versus model complexity for improving the performance of hydrological models in mountain catchments. *Water Resources Research*, 51(4):1939–1958.

Francke, T. (2002). Kurzbeschreibung zum Interpolationsmodul interpol v3. Available from developer upon request.

Francke, T., Foerster, S., Brosinsky, A., Sommerer, E., Lopez-Tarazon, J. A., Güntner, A., Batalla, R. J., and Bronstert, A. (2017a). Water and sediment fluxes in Mediterranean mountainous regions: Comprehensive dataset for hydro-sedimentological analyses and modelling in a mesoscale catchment (River Isábena, NE Spain). *Earth System Science Data Discussions*, 2017:1–17.

Francke, T., Foerster, S., Brosinsky, A., Sommerer, E., López-Tarazón, J. A., Güntner, A., Batalla, R., and Bronstert, A. (2017b). Hydro-sedimentological dataset for the mesoscale mountainous Isábena catchment. *GFZ Data Services*.

Francke, T., Güntner, A., Mamede, G., Müller, E. N., and Bronstert, A. (2008). Automated catena-based discretization of landscapes for the derivation of hydrological modelling units. *International Journal of Geographical Information Science*, 22(2):111–132.

Gafurov, A. and Bárdossy, A. (2009). Cloud removal methodology from MODIS snow cover product. *Hydrology and Earth System Sciences*, 13(7):1361–1373.

Gafurov, A., Kriegel, D., Vorogushyn, S., and Merz, B. (2013). Evaluation of remotely sensed snow cover product in Central Asia. *Hydrology Research*, 44(3):506–522.

Gafurov, A., Lüdtke, S., Unger-Shayesteh, K., Vorogushyn, S., Schöne, T., Schmidt, S., Kalashnikova, O., and Merz, B. (2016). MODSNOW-Tool: an

operational tool for daily snow cover monitoring using MODIS data. *Environmental Earth Sciences*, 75(14):1078.

Garbrecht, J. and Martz, L. W. (2000). Digital elevation model issues in water resources modeling. In Maidment, D. and Djokic, D., editors, *Hydrologic and Hydraulic Modeling Support with Geographic Information Systems*, pages 1–27. ESRI Press, Redlands, California, USA.

Garen, D. C. and Marks, D. (2005). Spatially distributed energy balance snowmelt modelling in a mountainous river basin: estimation of meteorological inputs and verification of model results. *Journal of Hydrology*, 315(1):126 – 153.

Garnier, B. and Ohmura, A. (1968). A Method of Calculating the Direct Shortwave Radiation Income of Slopes. *Journal of Applied Meteorology*, 7:796–800.

Gray, D. M. and Prowse, T. D. (1993). Snow and Floating Ice. In Maidment, D., editor, *Handbook of Hydrology*, chapter 7. McGray-Hill, Inc., New York, USA.

Green, W. H. and Ampt, G. (1911). Studies on Soil Phyics Part I - The flow of air and water through soils. *The Journal of Agricultural Science*, 4(1):1–24.

Grossi, G., Lendvai, A., Peretti, G., and Ranzi, R. (2017). Snow Precipitation Measured by Gauges: Systematic Error Estimation and Data Series Correction in the Central Italian Alps. *Water*, 9(7):461.

Güntner, A. (2002). Large-scale hydrological modelling in the semi-arid North-east of Brazil. *PIK Report No. 77, Institute for Climate Impact Research, Potsdam, Germany*.

Güntner, A. and Bronstert, A. (2004). Representation of landscape variability and lateral redistribution processes for large-scale hydrological modelling in semi-arid areas. *Journal of Hydrology*, 297(1-4):136–161.

Hall, D. K., Riggs, G. A., Salomonson, V. V., DiGirolamo, N. E., and Bayr, K. J. (2002). MODIS snow-cover products. *Remote Sensing of Environment*, 83(1):181 – 194.

Hay, J. E. and Mckay, D. C. (1985). Estimating Solar Irradiance on Inclined Surfaces : A Review and Assessment of Methodologies. *International Journal of Solar Energy*, 3:203–240.

Hock, R. (2003). Temperature index melt modelling in mountain areas. *Journal of Hydrology*, 282(1-4):104–115.

Hock, R. (2005). Glacier melt : a review of processes and their modelling. *Progress in Physical Geography*, 3:362–391.

Illangasekare, T., Walter, R., Meier, M., and Pfeffer, W. (1990). Modeling of Meltwater Infiltration in Subfreezing Snow. *Water Resoures Reasearch*, 26(5):1001–1012.

Knauf, D. (1980). Berechnung des Abflusses aus einer Schneedecke. In *Analyse und Berechnung oberirdischer Abflüsse*, pages 45–135. Schriftenreihe des DVWK Volume 46. Verlag Paul Parey.

Kneis, D. (2012). Eco-Hydrological Simulation Environment (ECHSE) - Documentation of model engines. University of Potsdam, Institute of Earth and Environmental Sciences. Available from: `http://echse.github.io/downloads/documentation/echse_engines_doc.pdf`.

Kneis, D. (2015). A lightweight framework for rapid development of object-based hydrological model engines. *Environmental Modelling & Software*, 68:110 – 121.

López-Tarazón, J., Batalla, R., Vericat, D., and Francke, T. (2009). Suspended sediment transport in a highly erodible catchment: The River Isábena (Southern Pyrenees). *Geomorphology*, 109(3):210 – 221.

Maleki, S., Hizam, H., and Gomes, C. (2017). Estimation of Hourly , Daily and Monthly Global Solar Radiation on Inclined Surfaces : Models Re-Visited. *Energies*, 10(134).

Monteith, J. L. (1965). Evaporation and environment. *Symp. Soc. Exp. Biol*, 19:205–234.

Moriasi, D. N., Arnold, J. G., Van Liew, M. W., Bingner, R. L., Harmel, R. D., and Veith, T. L. (2007). Model evaluation guidelines for systematic quantification of accuracy in watershed simulations. *Transactions of the ASABE*, 50(3):885–900.

Mueller, E. N., Güntner, A., Francke, T., and Mamede, G. (2010). Modelling sediment export, retention and reservoir sedimentation in drylands with the WASA-SED model. *Geoscientific Model Development*, 3(1):275–291.

Pan, X., Yang, D., Li, Y., Barr, A., Helgason, W., Hayashi, M., Marsh, P., Pomeroy, J., and Janowicz, R. J. (2016). Bias corrections of precipitation measurements across experimental sites in different ecoclimatic regions of western Canada. *The Cryosphere*, 10(5):2347–2360.

Parajka, J. and Blöschl, G. (2006). Validation of modis snow cover images over Austria. *Hydrology and Earth System Sciences*, 10(5):679–689.

Peschke, G. (1977). Ein zweistufiges Modell der Infiltration von Regen in geschichtete Böden. *Acta hydrophysica*, 22(1):39–48.

Peschke, G. (1987). Soil moisture and runoff components from a physically founded approach. *Acta hydrophysica*, 31(3/4):191–205.

Pilz, T., Francke, T., and Bronstert, A. (2017). lumpr 2.0. 0: an R package facilitating landscape discretisation for hillslope-based hydrological models. *Geoscientific Model Development*, 10(8):3001–3021.

Roy, A., Royer, A., and Turcotte, R. (2010). Improvement of springtime streamflow simulations in a boreal environment by incorporating snow-covered area derived from remote sensing data. *Journal of Hydrology*, 390(1):35 – 44.

Schulla, J. (1997). Hydrologische Modellierung von Flussgebieten zur Abschätzung der Folgen von Klimaänderungen. *Zürcher Geographische Schriften, Band 69, Geographisches Institut, Eidgenössische Technische Hochschule, Zürich, Switzerland, 161 pp.*

Sevruk, B. (1983). Correction of Measured Precipitation in the Alps Using the Water Equivalent of New Snow. *Hydrology Research*, 14(2):49–58.

Shuttleworth, W. J. (1992). Evaporation. In Maidment, D., editor, *Handbook of Hydrology*, chapter 4. McGray-Hill, Inc., New York, USA.

Shuttleworth, W. J. and Wallace, J. (1985). Evaporation from sparse crops-an energy combination theory. *Quarterly Journal of the Royal Meteorological Society*, 111(469):839–855.

Stisen, S., Højberg, A. L., Troldborg, L., Refsgaard, J. C., Christensen, B. S. B., Olsen, M., and Henriksen, H. J. (2012). On the importance of appropriate precipitation gauge catch correction for hydrological modelling at mid to high latitudes. *Hydrology and Earth System Sciences*, 16(11):4157–4176.

Tarboton, D. and Luce, C. (1996). Utah energy balance snow accumulation and melt model (UEB). Technical report, Utah State University and USDA Forest Service.

Tian, F., Sun, Y., Hu, H., and Li, H. (2016). Searching for an optimized single-objective function matching multiple objectives with automatic calibration of hydrological models. *Hydrology and Earth System Sciences Discussions*, 2016:1–33.

Tian, Y. Q., Davies-colley, R. J., Gong, P., and Thorrold, B. W. (2001). Estimating solar radiation on slopes of arbitrary aspect. *Agricultural and Forest Meteorology*, 109:67–74.

Walter, T. M., Brooks, E. S., McCool, D. K., King, L. G., Molnau, M., and Boll, J. (2005). Process-based snowmelt modeling: Does it require more input data than temperature-index modeling? *Journal of Hydrology*, 300(1-4):65–75.

Wang, X., Xie, H., and Liang, T. (2008). Evaluation of modis snow cover and cloud mask and its application in northern xinjiang, china. *Remote Sensing of Environment*, 112(4):1497 – 1513. Remote Sensing Data Assimilation Special Issue.

Zheng, Q., Chen, R., Han, C., Liu, J., Song, Y., Liu, Z., Yang, Y., Wang, L., Wang, X., Liu, X., Guo, S., and Liu, G. (2017). Correcting precipitation mea-

surements of TRwS204 in the Qilian Mountains, China. *Hydrology and Earth System Sciences Discussions*, 2017:1–20.